Construction and Building Materials 418 (2024) 135437

Contents lists available at ScienceDirect

Construction and Building Materials

journal homepage: www.elsevier.com/locate/conbuildmat

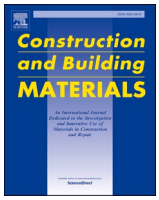

Ethyl silicate–nanolime treatment for the consolidation of calcareous building materials

Jing He [a], Jorge Otero [b], Laura Crespo-López [b], Luis Monasterio-Guillot [b,c], Cristina Benavides-Reyes [d], Kerstin Elert [b,e], Carlos Rodriguez-Navarro [b,*]

[a] School of Materials Science and Engineering (School of Conservation Science & Technology for Cultural Heritage), Key Laboratory of Materials and Technology for Unearthed Cultural Heritage Conservation, Ministry of Education, Shaanxi Key Laboratory of Green Preparation and Functionalization for Inorganic Materials, Shaanxi University of Science & Technology, Xi'an 710021, China
[b] Department of Mineralogy and Petrology, University of Granada, Granada 18002, Spain
[c] Univ. Grenoble Alpes, CNRS-ISTerre, Grenoble FR-38000, France
[d] Department of Operative Dentistry, University of Granada, Granada 18071, Spain
[e] Escuela de Estudios Árabes, Consejo Superior de Investigaciones Científicas (EEA-CSIC), Granada, Spain

ARTICLE INFO

Keywords:
Consolidation
Nanolime
Ethyl silicate
Biocalcarenite stone
Calcium Silicate Hydrate
Microstructure

ABSTRACT

Ethyl silicate (tetraethoxysilane, TEOS) is commonly used for consolidating construction materials containing siliceous components such as sandstone, cement mortars and concrete structures. This is especially due to its high compatibility with the substrates' silicate matrix. Its lack of bonding to calcareous substrates is however considered an important handicap. Here we investigate the consolidation effectiveness and durability of a combined TEOS-nanolime treatment applied on weathered biocalcarenite stone. We report evidence of physical and chemical interactions between the two consolidant materials resulting in limited drying shrinkage and the formation of calcium silicate hydrate (C-S-H) gel, responsible for improving the treated carbonate substrate mechanical properties and treatment durability as compared to both products used separately. The results of this experimental study are promising and could be the foundation for further studies toward obtaining a compatible, effective, and long-lasting consolidation treatment for porous calcareous building materials.

1. Introduction

Building materials (e.g., natural stones, cement/concrete, bricks and/or lime mortars) exposed to outdoor environments undergo several chemical, physical–mechanical and biological degradation processes that compromise their aesthetic appearance, internal cohesion and/or structural integrity [1,2]. Consolidants are commonly used to recover the strength of degraded building materials and decrease the substrate's deterioration rate (i.e., returning the properties of the decayed substrate as close as possible to those of the sound substrate) [3,4]. In general, suitable consolidants must meet the following criteria [1,3,4,5,6,7,8,9]: i) be physically, mechanically and chemically compatible with the substrate's main cementing material; ii) recover the substrate's mechanical properties; iii) reduce open porosity and capillary pores without creating a stark difference between the consolidated external layer and the inner core material; iv) reduce the capillary absorption rate without hampering the water vapor transport through the porous substrate; iv) not induce significant color or aesthetic changes such as generation of surface gloss; and v) maintain its effectiveness in the long-term. Additionally, the treated area must ideally have the same moisture and thermal expansion coefficient, and elastic modulus as the untreated material to avoid long-term internal stresses and assure complete compatibility [2]. Finally, in terms of practicality, the treatment also must be cost-effective, easy to apply and safe to handle, and meet national or regional health/safety and VOC (volatile organic compound) regulations.

Among consolidants, TEOS (tetraethoxysilane, $Si(OEt)_4$), also known as ethyl silicate, is one of the most commonly used products for consolidating siliceous-based construction materials such as sandstone, tuff stone, cement mortars and other concrete structures [2,7,10,11,12,13,14]. The popularity of TEOS products is due to their ample commercial availability and reasonable price, and their proven general high physical and chemical compatibility with siliceous materials, leading to a reduction in porosity and strength increase with minimal alteration in

* Corresponding author.
E-mail address: carlosrn@ugr.es (C. Rodriguez-Navarro).

https://doi.org/10.1016/j.conbuildmat.2024.135437
Received 29 November 2023; Received in revised form 2 February 2024; Accepted 10 February 2024
Available online 19 February 2024

substrate appearance [7,13]. Once applied to the substrate, ethyl silicate consolidates by means of a sol–gel process in a two-step mechanism [7,15]: *i)* first ethyl silicate undergoes hydrolysis in the presence of water (i.e., moisture and water vapor in the atmosphere or in the pores), forming reactive silanol groups (Si–OH) and ethanol, which evaporates leaving no residue; and *ii)* silanol groups polymerize by a polycondensation process forming siloxane bonds (Si-O-Si), and also reacting with OH-groups on the silicate surface. It precipitates within the porous substrate structure as amorphous silica gel, thus restoring the binding capacity of the cementing phase in the weathered substrate and reconnecting loose mineral grains, which ultimately leads to an increase in mechanical strength [2,7,13]. However, despite the advances in TEOS products and their widespread use for consolidating siliceous construction materials, they are also known to have some major drawbacks: i) important difference in thermal expansion coefficients of silica gel and other/common mineral phases [16]; ii) significant cracking due to drying shrinkage [17], and iii) poor consolidation effectiveness in carbonate-based substrates [7,18]. The difficulty in achieving a bond between ethyl silicate and carbonate-based substrates due to the absence of hydroxyl groups on the carbonate minerals' surface has long been considered an important problem, especially in architectural heritage conservation practice [1,7,18]. In general, it is claimed that the precipitated silica gel acts as a simple pore filler and creates an only weak physical bond with the substrate, resulting in limited improvement of mechanical properties and long-term durability [17,18,19]. To enhance compatibility and improve chemical bonding between ethyl silicate and carbonate substrates, different strategies have been proposed involving the use of coupling agents [2,7], addition of nanoparticles with anchoring capacity [19], or pre-treatments [20,21,22]. Ziegenbalg's group [22,23] explored the possibility of a combination of TEOS and nanolime in a series of preliminary investigations which involved: i) the application of a combined treatment of TEOS and nanolime in a homogeneous mixture; and ii) the consecutive application of nanolime dispersions (pre-treatments) followed by TEOS. Based on their preliminary findings, they reported that in both cases combined treatments were more effective in improving the mechanical properties and durability on several calcareous substrates than TEOS or nanolime separately. This improvement has been attributed either to enhanced gel formation due to the presence of hydroxide ions that catalyze the hydrolysis process, and/or a possible coupling agent capacity of nanolime [24]. Although the same group tested this strategy on several substrates using different treatment protocols, the underlying chemistry behind this combined treatment remains poorly understood. Advances in cement and concrete composites have evidenced improved performance of ethyl silicate consolidants in combination with slaked lime [11] or nanolime particles [25] through the precipitation of additional calcium silicate hydrate (C-S-H) gel upon pozzolanic reactions between ethyl silicate and $Ca(OH)_2$ (nano)particles, as well as with portlandite crystals formed during cement hydration [26,27]. As a result, a significant densification and strengthening of the cement material occurs, while conserving the original color and appearance. Borsoi et al. [28] and Matos et al. [29] reported appropriate consolidation of lime renders following the application of TEOS plus lime water or nanolime, respectively, yet the authors do not report C-S-H formation. Michalopoulou et al. [30], in contrast, observed that a limited formation of C-S-H occurs upon reaction (at room *T*) of TEOS and nanolime. It is evident that further research on the effectiveness, strengthening effect, and underlying chemistry of mixed TEOS-nanolime consolidants is needed, particularly considering the sometimes-conflicting results regarding their *modus operandi* and effectiveness [31]. Based on the current knowledge, we hypothesized that the above-mentioned "pozzolanic effect" could be partly responsible for the successful results observed in Ziegenbalg's preliminary experiments [22]. However, other effects might be at play and a better in-depth understanding of the technology could enable the design of improved TEOS-nanolime consolidants, for their use as compatible, effective, and long-lasting consolidation treatments for calcareous building materials.

Here we explore the effectiveness and durability of a combined TEOS-nanolime treatment applied on a calcareous substrate (biocalcarenite stone). Concrete/cement composites were not considered here as inherent C-S-H could mask the effect of the treatment, foster the heterogeneous precipitation of consolidant-based C-S-H (i.e., seed effect), or promote pozzolanic reactions between the TEOS-derived silica gel and the portlandite formed upon cement hydration [11]. The textural, physical, hydric, and mechanical properties of treated calcareous stone samples were determined and compared to control samples and samples treated with either ethyl silicate or nanolime. The outcome of this study not only provides an in-depth understanding of underlying reaction mechanisms in TEOS-nanolime mixtures and shows a new pathway for the formation of C-S-H, it also offers valuable information to conservation specialists aimed at improving treatment protocols and designing optimized consolidants for heritage conservation.

2. Materials and methods

2.1. Calcareous stone

The selected stone is a biocalcarenite from San Cristóbal (El Puerto de St. Maria, Cádiz, Spain), which has been extensively used in heritage buildings in the south of Spain, including the Cathedral of Seville [10]. San Cristobal biocalcarenite stone is characterized by having a sparitic carbonate cement (carbonate particles larger than 2 μm), as well as calcite bioclasts, along with quartz (large aggregates) and feldspar grains [10,32]. Additional minerals such as phyllosilicates and zircon are also commonly present in this stone in minor amounts [32]. For our experiments, a large block coming from the quarry was cut into 40 ×40 ×40 mm cubes for testing. The mineralogical composition was determined by X-ray diffraction (XRD, PANalytical XPert PRO) with Cu Kα radiation and Ni filter. XRD patterns were recorded with a step size of 0.026 °2θ and goniometer speed of 0.05 °2θ s^{-1}, in the angular range 3–70 °2θ. Crystalline phases were identified by comparison of experimental XRD patterns with those published in the International Center for Diffraction Data (ICDD) reference database, and their semi-quantification was performed using the reference intensity ratio (RIR) method [33]. XRD semiquantitative RIR analysis shows that this stone includes calcite as the main phase (50%, $CaCO_3$, ICCD card #83–0577), with a relatively large amount of quartz (35%, SiO_2, ICDD card #83–0539) and small amounts of feldspar (15% microcline, $KAlSi_3O_8$, ICCS card #22–0687) (see Supplementary Material, Fig. S1). The pore structure was determined by mercury intrusion porosimetry (MIP) by means of an Autopore 9600 (Micromeritics) instrument equipped with low- and high-pressure cells, the latter reaching 30,000 PSI (207 MPa). Samples for MIP consisted of stone fragments (~1 g) which were dried in a ventilated oven at 60 ºC until constant weight, i.e., when three successive measurements showed a weight variation <1% after >24 h (up to 48 h). A moderate *T* of 60 °C was selected (instead of standard 110 °C) to enable a comparison with treated samples, which were dried at 60 °C (see below) to avoid/minimize heat-related changes in the consolidants. MIP results show that the open porosity of this stone is 29 ± 3% ($N = 2$) with a bulk density of 2.04 ± 0.11 g cm^{-3} ($N = 2$).

2.2. Weathering of stone blocks prior to consolidation

To evaluate the effect of the consolidation treatments, stone samples were first artificially weathered (labeled as "W"), as recommended by NORMAL 20/85 when evaluating the effectiveness of consolidation treatments in construction materials [34]. Note that 3 additional cube-shaped specimens were kept without weathering as control samples (labeled as "CO"). Artificial weathering was performed by creating damage through several salt crystallization cycles (15 cycles) according to EN 12370 [35]. This experiment followed the recommendations stated by Lubelli et al. [36] including the use of non-destructive

techniques (NDT) such as ultra-sounds pulse velocity (UPV) to monitor the decay, and the measurement of conductivity at the end of the crystallization cycles to ensure that no residual salt remains in the samples after the weathering process. Here UPV was measured using a Control 58-E4800 portable tester (with transducers of 54 kHz and a circular contact surface of 27 mm in diameter) following ASTM D2845 [37]. P-wave velocity values (*Vp*) decreased from 1610 ± 32 m s^{-1} ($N = 12$) to 1344 ± 50 m s^{-1} ($N = 12$), indicating a reduction in the material's stiffness or elastic modulus upon weathering. Conductivity values decreased significantly from an initial 52.718 mS cm^{-1} to less than 0.001 mS cm^{-1}, which confirms that desalination by repeated immersion in deionized water was complete at the end of the weathering test. The open porosity (MIP) of weathered samples was 31.7 ± 2.0% ($N = 2$) and the bulk density 2.18 ± 0.19 g cm^{-3} ($N = 2$).

2.3. Consolidation products

Two commercial consolidation products and a mixture of both were used:

(i) CALOSIL E25® (IBZ Salzchemie GmbH & Co.KG, Germany): 25 g L^{-1} calcium hydroxide in ethanol. Particle size 50–150 nm. This product has a density of 0.80 g cm^{-3} (at 20 ºC) and a viscosity of 0.00275 kg m^{-1} s^{-1}) (at 25 ºC) according to the manufacturer. This nanolime dispersion is referred to as C.

(ii) ESTEL 1000® (CTS, Spain): 75 wt% ethyl silicate (40% monomers, 35% dimmers/trimers, also containing 1% dibutyltin dilaurate as a catalyst) and 25 wt% white spirit. This product has a density of 0.97 g cm^{-3} (at 20 °C) and a viscosity of 0.0049 kg m^{-1} s^{-1}) (at 25 ºC) according to the manufacturer. This consolidant is referred to as T.

(iii) Mixture of CALOSIL E25® and ESTEL 1000® in a 1:3 vol ratio (see details below). The two products were mixed and sonicated for 30 s right before application onto the porous stone. This mix is referred to as CT and has a Ca/Si mole ratio of 0.04. This mixture was selected after extensive preliminary testing considering the curing and textural/structural evolution at different mixing ratios. C:T ratios > 1:3 led to inhomogeneous white silica gel products (Fig. S2). Additionally, such mixes led to excessive dilution of the T component, leading to a TEOS-depleted consolidant, which might jeopardize the effectiveness of the treatment. Conversely, C:T ratios < 1:3 resulted in amorphous silica gel films displaying pervasive cracking due to drying shrinkage [7], also noted in our preliminary experiments where cracks were more abundant as the concentration of T in the mix increased (up to 57±5 cracks/mm^2 for pure T as shown by SEM imaging) (Fig. S2a). Therefore, a 1:3 vol ratio of C and T was selected as it led to just a 25% dilution of the TEOS component and a lower amount of drying cracks (40±13 cracks/mm^2) (Fig. S2b), and provided an optimal amount of $Ca(OH)_2$ to maintain a high pH for alkaline catalysis of TEOS hydrolysis (see below).

2.4. Consolidation treatment

Weathered stone samples (blocks) were treated with (i) C, (ii) T, and (iii) CT. Each of these treatments was applied to 3 cubic weathered stone specimens (Fig. S3a-b). Note that 3 weathered samples were kept without the application of any consolidation treatment (labeled as W) to be compared to CO and treated samples. The lateral faces of each cubic sample were sealed with parafilm to avoid the ingress of the product (Fig. S3b) [38,39].

The treatment was applied to the cubic samples under laboratory conditions ($T \approx 20$ ºC and ≈ 50% RH) by brushing only on one face, which was placed vertically (i.e., the treated face, Fig. S3c). The brushing was continued until the consolidant reached the opposite side of the sample, achieving full saturation (typically after ≥40–60 strokes). Product absorption was monitored during treatment application and the application process was stopped when no further absorption was observed (the weight increase reached asymptotic values, with a weight variation <1% between successive measurements) (Fig. S3d). This application procedure has been successfully used in previous consolidation treatments [12,40]. Samples were weighed before and right after saturation, yielding a final average weight increase of 10±0.3, 12±0.3, and 13±2.4% for the C, T and CT treatments, respectively. After treatment application, samples were cured in a climate chamber for a period of 8 weeks ($T \approx 20$ °C, RH ≈ 60–70%; Fig. S3e). The two months curing period was selected as a compromise between the time needed for hydrolysis and polycondensation of TEOS, and a practical time for further testing and analysis. The untreated weathered specimens and the control samples were also stored under the same conditions.

2.5. Consolidation effectiveness

Following the two-month curing in the climate chamber, the biocalcarenite cubes were dried to constant weight at 60 ºC in a ventilated oven and subsequently stored in a desiccator until further testing.

Changes in the surface appearance of the treated stone samples were visually evaluated using an optical microscope (Wild M8, with 20x objective). Any possible treatment-related color changes were determined with a spectrophotometer (Minolta CM508D Colorimeter) using the CIE$L^*a^*b^*$ color space, illuminant D65, 10° observer, and 8 mm diameter aperture [41]. Thirty readings were taken on different sample areas. Total color variation (ΔE^*) is calculated by the formula:

$$\Delta E^* = \sqrt{\Delta L^{*2} + \Delta a^{*2} + \Delta b^{*2}} \quad (1)$$

where ΔL^* is the change in luminosity (white-black parameter), Δa^* (red-green parameters) and Δb^* (blue-yellow parameters).

Differences in pore size distribution and open porosity were measured by MIP. Tests were carried out on two samples collected from the surface (up to a depth of 10 mm) of each of the treated samples and compared to control and unconsolidated weathered samples. Two additional samples were collected from the interior of the treated samples, one from the middle (between 10 and 20 mm depth from the surface) and one from the bottom areas (between 20 mm to bottom) to study the penetration of each of the treatments.

The "Scotch tape" or peeling test was used to evaluate changes in surface cohesion upon consolidation according to ASTM D3359 [42], also included elsewhere [43]. The test was carried out on treated, weathered and control samples with a mean of 9 measurements for each testing condition.

The increase in surface cohesion after treatment was also evaluated by means of a portable Leeb hardness tester (PCE-2500 N, PCE Instruments, Germany) [44,45]. For this test, the surface hardness Leeb value (HLD), where D is the indenter type, was calculated as an average of at least 15 points. Average HLD values were used to calculate differences among testing conditions and compared to control samples.

An Instron 3345 equipment (Instron Co., Canton, US) was used to determine variations in tensile and compressive strength upon consolidation following EN 1015–11 [46]. Prismatic samples (30 × 9 ×9 mm) were prepared for mechanical testing. Nine prisms were cut from each of the untreated and treated cubes, which were first cut in three equal-sized slices (top, middle, bottom, the top slice corresponding to the treated face), and then from each slice, three equal-sized prisms were cut using a low-speed diamond saw (see schematic of the sample preparation/cutting in Fig. S4). A load of 5000 N at 3 mm min^{-1} was applied to at least 6 specimens per testing condition. First the tensile strength was determined using the three-point bending test, and the resulting two pieces after fracturing were used for the uniaxial compressive test. Note, however, that here we only discuss the results of the flexural strength test, as the unconfined compressive strength (UCS) test yielded inconsistent results with a very large standard deviation, which precluded us from gathering any meaningful conclusion regarding this mechanical property. Indeed, it was observed that the weathered stone samples showed higher UCS values (nearly double) than those of the unweathered ones, which is unreasonable and casts doubts about the reliability

of the results obtained for this test. This is likely due to possible non-parallelism/excessive surface roughness of the tested specimens. This is not apparently an issue in the case of the three-point bending tests, as the contact area during testing is minimal.

A drilling resistance measurement system (DRMS, SINT-Technology, Italy) was used to measure the variation in mechanical strength along a depth profile and to estimate the penetration depth of consolidants [47,48]. Tests were performed on treated and back faces of control, weathered, and treated samples using a 5 mm diameter diamond-tip drill bit, a rotation speed of 400 rpm, a penetration rate of 15 mm/min and a penetration depth of 30 mm. Drilling resistance (DR) average values and standard deviation were calculated as the mean of 6 tests per treatment/specimen.

Strength improvement after treatment application was also evaluated using UPV measurements, which is a non-destructive technique that can be applied in situ. Measurements were carried out on three samples per testing condition, following ASTM D2845 [37].

Water absorption coefficient (WAC) and capillary absorption (sorptivity) curves were obtained according to EN 13755 on three control and three treated samples per testing condition [49]. Upon completion of this test, the samples' open porosity was calculated following water saturation under vacuum following ASTM C67–00 [50]. The samples' drying behavior was calculated according to EN 16322 [51]. This testing procedure is fully described elsewhere [52].

The water vapor permeability (WVT) was evaluated on treated samples (Ø = 2.5 cm and height = 1 cm) using the procedure described in Charola et al. [52]. Cylindrical containers (Ø = 2.5 cm and height = 7 cm) were filled with cotton wool and 5 mL saturated KNO_3 solution to maintain 93% RH inside the container. The seal between the sample and container was obtained using plasticine covered by Parafilm®. Samples were kept in a desiccator with silica gel at <5% RH (room *T*). The weight loss over time was measured at predetermined time intervals. From these data, the WVT rate (WVTR) was determined as the mass change per unit time and surface area of the stone samples (with 1 cm thickness). The measurements were carried out on three samples per testing condition.

To further evaluate the effectiveness of consolidation treatments and possible surface hydrophobicity, the sessile drop method was applied to determine the static contact angle of 4 μL water drops deposited on the surface of the treated face and compared to control samples using an OCA 15 EC equipment (Data Physics Instruments, Germany) following UNE-EN 828 [53]. Average values are based on at least 3 measurements per testing condition.

Textural and compositional characteristics of carbon-coated samples (a cross-section per testing condition) were studied using field emission scanning electron microscopy (FESEM, AURIGA, Carl Zeiss, Germany) coupled with energy dispersive spectrometry (EDS, INCA-200, Oxford Instruments, UK). Equipment settings: 3 kV acceleration voltage in secondary electron imaging mode and 20 kV acceleration voltage for EDS microanalysis.

To evaluate the long-term performance of T and CT treatments, consolidated samples were subjected to the salt weathering test described above. Evaluation using DR measurements was limited to T and CT treatments because these showed a higher degree of consolidation in terms of mechanical properties and porosity reduction than the nanolime treatment, which had a very limited consolidation effect when applied to this stone type (see Section 3).

Finally, to identify the possible formation of C-S-H in CT treatments, analyses were performed involving the study of the spectral and ultrastructural/compositional features of the reaction products formed after curing of CT deposited on Petri dished and cured at room *T* (20° C) and 75% RH for at least one month. For this task, the cured CT solids were ground in an agate mortar and subsequently analyzed by Fourier transform infrared spectroscopy (FTIR, JASCO 6200 equipped with a diamond-typed attenuated total reflectance, ATR unit, 400–4000 cm^{-1} spectral range, and 4 cm^{-1} spectral resolution), thermogravimetry coupled with differential scanning calorimetry (TG-DSC, Mettler-Toledo, TGA/DSC1, analyses performed in 50 mL min^{-1} flowing air, using alumina crucibles, 20–40 mg sample mass and 10 K min^{-1} heating rate), and transmission electron microscopy (TEM, FEI Thalos, with acceleration voltage of 200 kV, and equipped with a high angle annular dark field detector, HAADF) coupled with energy dispersive X-ray spectrometry (EDS) microanalysis. EDS point and area (2D) compositional analyses were performed in scanning TEM mode (STEM). Prior to TEM analysis the powder samples were dispersed in ethanol and sonicated for 2 min. The dispersed powder was fished with carbon-coated Cu TEM grids, which were introduced in the TEM sample holder for analysis. XRD analysis of the CT product before and after thermal treatment (heating for two hours at 950 °C) was also performed (using the equipment and analytical protocol above described). The thermal treatment was performed to disclose whether C-S-H was present in cured CT, as in [11].

3. Results and discussion

3.1. Effect of the treatments on stone appearance

Fig. 1 shows representative optical microscopy images of the treated samples' surface. It is observed that salt weathering did not result in a significant change in color, but the surface roughness increased as compared with the unweathered control (Fig. 1a and b), and some large pores (due to loss of surface material) developed. Rounding of the samples edges and corners was also observed (Fig. S5). These observations show that the adopted ageing protocol was effective in inducing damage. The nanolime treatment (C) led to a whitening effect (Fig. 1c), despite the fact that right after treatment application excess surface nanolime was removed with a wet cloth, as recommended by López-Martínez and Otero [54]. The other two treatments, TEOS (T) and nanolime-TEOS (CT), produced no detectable changes in the surface appearance (Fig. 1d and e). Color change after C treatment was even more dramatic if the excess surface consolidant was not eliminated as shown in Fig. 1e. These visual observations were confirmed by spectrophotometric measurements (Table 1). The TC treatment resulted in ΔE^* values < 3, which are not detectable by the human eye. The treatment with T led to ΔE^* values slightly over 3, but still below $\Delta E^* = 5$, which is considered the acceptable threshold for a consolidation treatment [6]. Conversely, the C treatment resulted in $\Delta E^* > 5$, which is not acceptable in heritage conservation. Such a significant color variation is due to a change in the L^* (increased lightness) and b^* (towards more negative values, i.e., blue component) parameters. Note that the surface accumulation of nanolime and associated color changes have been observed after the application of this treatment on different porous substrates and are generally related to back migration of the nanolime particles during solvent (alcohol) evaporation [55,56].

3.2. Changes in porosity and pore size distribution

Table 2 shows the results of the MIP analysis of untreated and treated samples. As indicated above, the salt weathering test led to an increase in the stone porosity from ~29% up to ~32%. However, the large data spread in measured porosity values precludes us from drawing any sound conclusion on the effect of the salt weathering test in stone porosity. Still, the observed increase in surface roughness (see above) clearly points to material loss and creation of porosity on the weathered stone surface, which underlines the effectiveness of such an ageing process. Indeed, it enables obtaining in a rapid way stone samples reflecting the damage they would have suffered *in situ* (i.e., in a monument) [57,58,59]. Note that several studies on the effectiveness of consolidants typically use non-weathered quarry stones, which may not be the best choice to evaluate the behavior of a consolidation treatment in a real-case scenario [59]. The three treatments induced a marked reduction in open porosity (i.e., accessible to Hg), from 31.7% (W) to

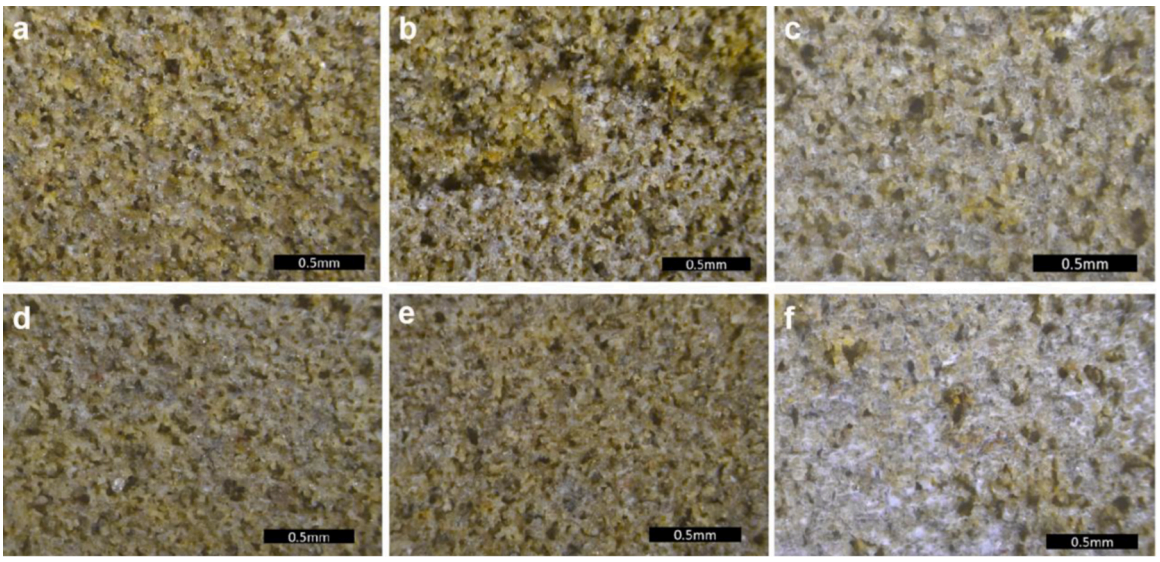

Fig. 1. Microscope images of the untreated and consolidated samples' surface. a) untreated control (CO); b) untreated control after salt weathering (W); c) sample treated with nanolime (C). Removal of the surface excess consolidant right after treatment application (using a wet cloth) was performed; d) T; e) CT; and f) C treatment without removal of surface residue.

Table 1
Chromatic alterations for treated samples as compared to the untreated control.

Treatment	ΔL^*	Δa^*	Δb^*	ΔE^*
C*	3.94	-1.12	-6.50	7.68
T	-3.04	0.88	1.66	3.57
CT	-2.01	-0.41	-0.64	2.15

* Treatment involving removal of surface excess consolidant

Table 2
Open porosity of untreated and treated samples determined by mercury intrusion porosimetry and water absorption under vacuum (N=2) of samples taken from the top, middle, and bottom.

	Porosity (%)	MIP Average	Std dev	Water Average	Std dev
CO		29.1	±3.1	30.9	±1.5
W		31.7	±2.0	29.9	±0.2
Ctop	25.6				
Cmid	21.2	22.9	±2.4	29.8	±0.4
Cbot	21.8				
Ttop	20.2				
Tmid	18.2	18.3	±1.9	25.0	±0.3
Tbot	16.5				
CTtop	22.1				
CTmid	20.6	19.9	±2.6	28.4	±2.2
CTbot	17.1				

18.3%, 22.8% and 19.9%, for T, C, and CT treatments, respectively, values significantly lower than that of the unweathered control (29%). Note that these values represent averages derived from samples taken at three different depths. However, it is important to emphasize that while the trend was similar, open porosity values determined for the treated samples by water saturation under vacuum were higher than those obtained by MIP (Table 2). The reason for this outcome is not fully clear, although it could be argued that unlike water (under vacuum), our MIP equipment (reaching only 207 MPa in the high-pressure cell) could not fill the smallest pores in these samples (i.e., gel pores resulting from the TEOS-based treatments) [60], therefore yielding lower open porosity values. Note that previous studies of cement mortars and pastes also observed lower porosity values for MIP as compared with water absorption due to the limitations of the former technique to reach meso and micropores [61,62].

Consolidant accumulation along the top to bottom profile of the samples, leading to variations in open porosity, was treatment-dependent (Table 2 and Fig. 2): (i) samples treated with C presented lower porosity in the top than in the middle and bottom areas, implying treatment accumulation at the treated surface or near-surface, and limited penetration (Fig. 2a). This is consistent with the observed color change (see above) associated with surface accumulation of the nanolime consolidant due to back migration during solvent (ethanol) evaporation [55], one of the main handicaps of this consolidant [56]. Nonetheless, the reduction in porosity along the depth profile, reaching values similar or lower than those of the unweathered control (CO) shows that (a limited amount of) newly-formed $CaCO_3$ was deposited in-depth after carbonation of $Ca(OH)_2$ nanoparticles [63,64,65]; (ii) samples treated with T also showed lower porosity in the top part than in the middle and bottom areas (Fig. 2b). In this case the porosity reduction, especially in the top part, was significant, implying that a large volume of silica gel deposited/filled the pores; (iii) in contrast, samples treated with CT showed a higher porosity reduction in the middle and, specially, bottom areas (Fig. 2c). This was unexpected and suggests that the combination of nanolime and ethyl silicate favors penetration. In the latter two cases, the volume of solids introduced/deposited within the stone pores after treatment was higher than in the case of the nanolime treatment. This is consistent with the fact that the mass % of TEOS per unit vol of consolidant solution was higher (T treatment: 75 wt% in ESTEL1000®; CT treatment; 56.3 wt% TEOS plus 0.63 wt% $Ca(OH)_2$) than that of the nanolime dispersion (2.5 wt% in CaLoSiL®E25).

The biocalcarenite stone displayed an unimodal pore size distribution (PSD), with a maximum at ~40 μm. After treatment, partial filling of pores with size < 20 μm occurred in all cases (Fig. 2). This is generally observed after consolidation of porous stones [2,10,14,66]: i.e., the smallest pores tend to be preferentially filled, and their vol% is therefore reduced. This is considered a desirable effect of a consolidation treatment [66], as the smallest pores (diameter < 1–5 μm) typically favor weathering processes such as salt damage [67,68].

3.3. Surface strengthening

Peeling tape test results are shown in Table 3. Weathering resulted in a significant increase in surface loss, further underlining the effectiveness of the adopted ageing process. After treatment with C and T, the loss

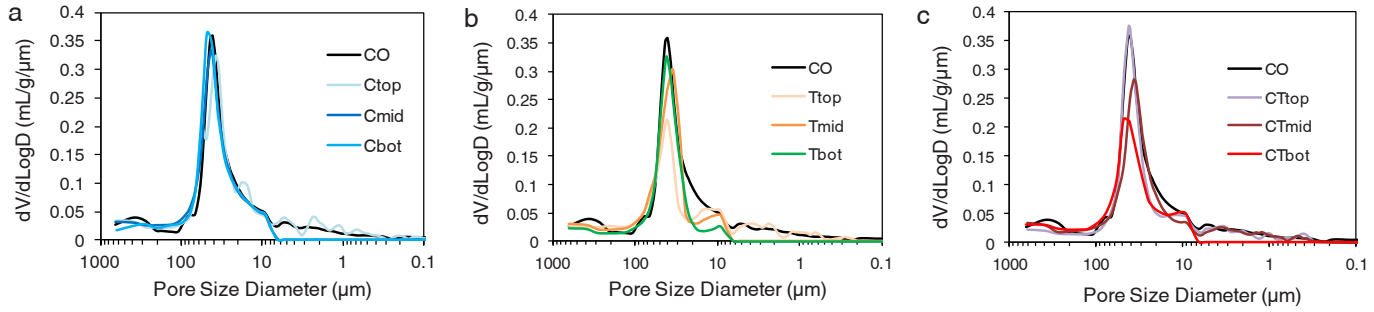

Fig. 2. Pore size distribution (from MIP analysis) of untreated and treated biocalcarenite samples. a) Treatment with Calosil (C); b) treatment with TEOS (T); and c) treatment with Calosil-TEOS (CT). Each graph shows the control (CO) as reference; top, mid and bot indicate the pore size distribution of samples collected from the top, middle and bottom parts of treated samples, respectively. The pore size distribution of W is not included due to its similarity to the control.

Table 3
Scotch tape test results (standard deviation included) for the surface of untreated and treated surfaces.

Treatment	Removed material (mg cm^{-2})	Variation (%)
CO	8.7 (1.89)	-
W	33.6 (17.92)	286.20
C	13.3 (7.01)	52.71
T	8.9 (4.87)	2.02
CT	6.7 (2.58)	-23.18

of surface material was reduced to values close to those of the unweathered control. Only in the case of the CT treatment the loss of surface material was significantly reduced as compared with the unweathered control, indicating that this treatment was able to effectively cement surface grains to a level slightly higher than that of the undecayed material.

Fig. 3a shows the results of the Leeb surface hardness test, indicating a large reduction in HLD values after the weathering tests and an increase after treatment to values close to or above those of the unweathered stone. In the case of the C treatment, surface hardness increased as compared with the weathered material, even though, the final average HLD value was below that of the unweathered control. In the case of the T treatment, the weathered stone regains the original value of the unweathered material. Finally, an increase in surface hardness of 10% as compared with the unweathered control is observed after the CT treatment. These results are consistent with those of the scotch tape test and corroborate that the CT treatment is the one that provides the highest surface strengthening. However, a surface strengthening effect *per se* is not a demonstration of treatment

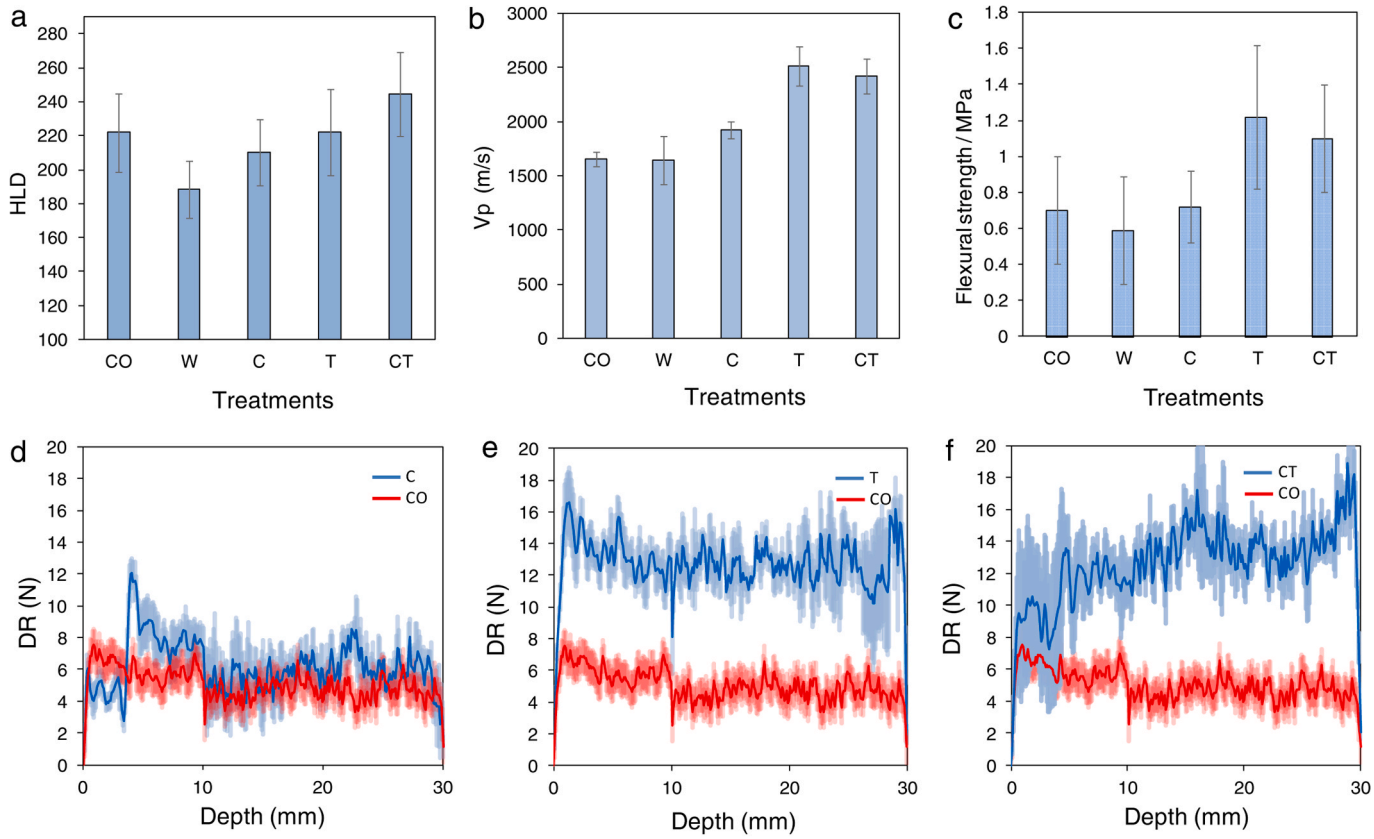

Fig. 3. Physical-mechanical properties of untreated and treated samples: a) Leeb surface hardness (HLD). The surface hardness was measured on the treated surface; b) *Vp* values; and c) Flexural strength; d-f) Drilling resistance (DR) of samples treated with (d) C, (e) T and (f) CT (blue curves) compared with the untreated control (red curves). Shaded areas show standard deviation.

effectiveness, as this effect could simply be due to the formation of a hardened thin surface layer, which would be detrimental to the long-term behavior of the treated substrate [69]. This is why it is necessary to also evaluate the in-depth strengthening effect of consolidation treatments, as shown in the following section.

3.4. Changes in mechanical properties

To evaluate the changes in dynamic mechanical properties of stone samples following treatment, we performed *Vp* measurements. The results are presented in Fig. 3b. The *Vp* values of the weathered control samples were slightly lower than those of the unweathered control. This was unexpected, considering the surface degradation observed after the weathering test. This could likely be due to both the heterogeneity of this stone and the fact that salt damage during crystallization cycles tends to concentrate on the surface and near surface areas of porous stone samples, primarily resulting in granular disintegration and sanding and/or scaling [67]. As such, the core of the sample would remain rather unaffected by salt damage, explaining the very small reduction in *Vp* experienced by the bulk stone. Conversely, all the treatments increased *Vp* to values above those of the unweathered control, with T showing the highest increase in *Vp*. However, the difference among T and CT treated samples is not significant (i.e., within error).

Table 4 shows the values of flexural strength (FS) and uniaxial compressive strength (UCS) of the untreated and treated stone samples. As stated in the Materials and methods section, UCS values were inconsistent and unreliable. Therefore, although they are reported in Table 4 for completeness, they are not further discussed. Note that nine prismatic pieces (3×0.9×0.9 cm) were extracted from each sample: 3 corresponding to the top, 3 to the middle and 3 to bottom part (Fig. S4), which were subjected to mechanical testing. This, in addition to obtaining an average bulk FS for each sample, enabled us to gather an insight on the effect the penetration and distribution of the different consolidants within the pore system of the stone has on the mechanical properties of treated stones.

After weathering, samples presented slightly lower flexural strength (0.59 MPa) as compared to the control (0.70 MPa) (Table 4 and Fig. 3c). Weathered samples treated with C (0.72 MPa) were able to regain the FS values of unweathered CO samples, whereas T and CT samples showed a significant increase in average FS of up to 74% (1.22 MPa) and 57% (1.10 MPa), respectively, as compared with the unweathered control. It should be indicated that an increase in strength of >50% after treatment is not recommended, as it might create an excessively hardened surface layer [2]. In this respect, the T treatment seems to be less compatible than the CT treatment in terms of strengthening. The large increase in flexural strength achieved with the T treatment suggests that the treatment did not only act as a pore filler, but likely established a strong bonding with the silicate minerals (quartz and feldspar) present in the stone. As to the effect of penetration on FS, samples treated with C presented a slightly higher average strength of the surface layer, whereas samples treated with CT showed a slightly higher strength in the mid and bottom areas, in both cases consistent with MIP results, and no clear trend was observed in the case of T-treated samples. Yet, in all cases, the differences were within error, which precludes drawing any sound conclusion about the change in FS with depth associated with treatment penetration and the degree of cementation.

Table 4
Flexural strength (FS) of untreated and treated stone samples.

	FS (MPa)	std dev	UCS (MPa)	std dev
CO (bulk)	0.70	0.3	5.85	2.1
W (bulk)	0.59	0.3	10.2	6.7
C (bulk)	0.72	0.2	12.2	5.9
surface	0.81	0.1	10.11	5.0
middle	0.69	0.2	14.60	6.1
bottom	0.68	0.1	11.74	6.7
T (bulk)	1.22	0.4	6.2	2.4
surface	1.09	0.5	4.87	2.9
middle	0.97	0.2	7.31	3.0
bottom	1.48	0.3	6.46	1.3
CT (bulk)	1.10	0.3	8.8	5.6
surface	0.90	0.2	4.41	2.2
middle	1.24	0.5	8.92	5.2
bottom	1.16	0.2	12.99	9.3

More conclusive evidence regarding treatment penetration and associated strength variation along a depth profile was obtained with DR tests (Fig. 3d-f). Samples treated with C presented a slight increase in DR (average value along the depth profile of ~8.3 N) as compared with the control (~5 N), with a more marked increase at ~4 mm depth. Conversely, samples treated with T (~12.6 N) and CT (~12.6 N) showed a significant increase in DR all along the depth profile. In the case of the CT treatment, DR values continuously increased along the depth profile, reaching peak values higher than those of the samples treated with C or T. The observed increase in DR with depth for the CT treatment is in full agreement with MIP results and demonstrates that this treatment does not result in a detrimental hardened surface layer.

3.5. Water behavior

Fig. 4a and 4b show the water absorption and drying curves, respectively, of the untreated and treated samples. CO, W and C samples absorbed water at a similar and very fast rate (WAC of 0.037 ±0.004 g cm^{-2} s$^{-0.5}$), and a similar volume (within error) at the end of the test (after 7 days). This shows that the salt weathering aging or the treatment with nanolime have no significant impact on the samples' water behavior. Conversely, T and CT treatments drastically altered the water absorption behavior of the stone. The T treatment resulted in a very marked reduction of the water absorption rate during the first 34 h (0.0004±0.0001 g cm^{-2} s$^{-0.5}$). Subsequently, the rate increased (0.0020±0.0002 g cm^{-2} s$^{-0.5}$), reaching values of saturation lower but close to those of the control (CO and W) after 7 days, a behavior previously observed following application of TEOS to porous stone and caused by transient hydrophobicity due to incomplete hydrolysis of ethoxide groups and further hydrolysis upon long-term contact with water [1,12,70]. The initial very low water absorption rate could also be due to pore clogging, yet MIP results show no drastic change in PSD (Fig. 2b). The fact that the final water absorption in T-treated samples reaches values very close to those of the control is apparently inconsistent with the observed porosity reduction after T treatment detected with MIP. It should be noted, however, that the values of porosity of T samples determined by forced water absorption under vacuum were higher than those of MIP and approached the values of the control (Table 2). Hence, it is likely that the delayed saturation is not solely due to a change in contact angle following enhanced hydrolysis of TEOS as claimed by Franzoni et al. [70], but also due to the difficulty of accessing the smallest pores, that is, the gel pores (2–10 nm) present in the silica gel formed after TEOS [71], which were eventually accessed by water but not by Hg using our MIP equipment.

The change in the water absorption rate of CT-treated samples, from a short initial period of fast absorption to a nearly constant low absorption rate (0.0063±0.0019 g cm^{-2} s$^{-0.5}$), not reaching saturation over the time-span of the test (7 days), is likely due to the presence of a fraction of not yet hydrolyzed TEOS in the interior of the samples [69] and abundant nm-sized pores in the silica plus C-S-H gel (see following section) formed after CT treatment. Note that the capillary absorption rate or sorptivity (i.e., water flux within the pores) is proportional to pore size [72]. This means that the water flux is reduced by the presence of nanopores (i.e., gel pores).

It is important to underline that the sorptivity modifications brought about by T and CT treatments do not negatively affect the drying behavior of the samples (Fig. 4b). They reach a full dry state at the same time as the control (weathered and unweathered) and the samples treated with nanolime. This is considered a positive effect of all the

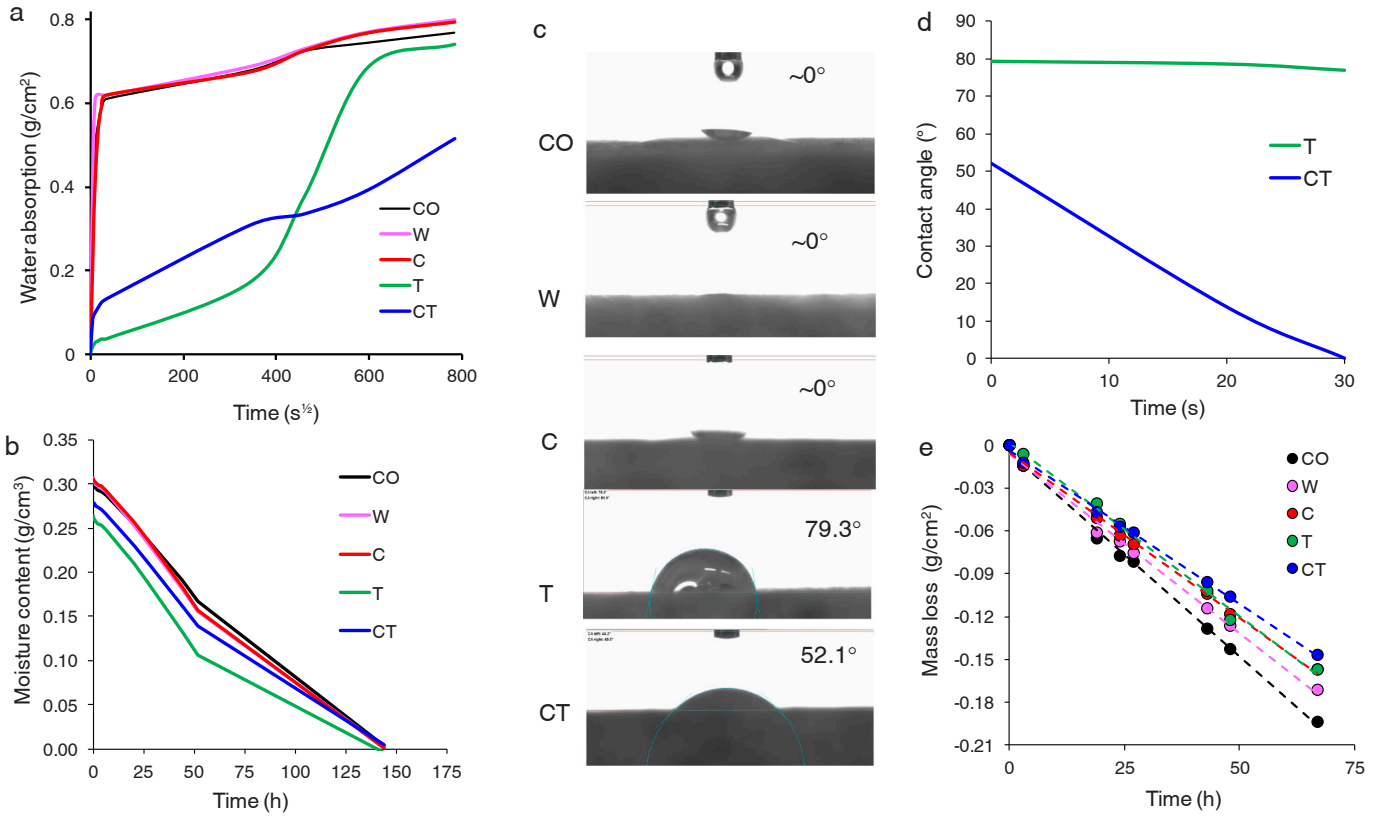

Fig. 4. Water behavior of untreated and treated stone samples. a) Free water absorption; b) Drying; c) Static contact angle; d) Time evolution of the contact angle of water drops deposited on stone samples treated with T and CT; e) Mass loss of samples subjected to the water vapor permeability test.

applied treatments [2,5].

To further understand the water behavior of the treated samples we measured the static contact angle. Fig. 4c shows images of the 4 μL water drops deposited on each substrate. In the case of the control (weathered and unweathered) and C-treated samples showed a contact angle of ~0°, meaning that the nanolime treatment did not seem to have affected the hydrophilic nature of the substrate. Conversely, T and CT treatments induced a marked increase in contact angle (up to 79° and 52°, respectively). Yet, while in the case of T the contact angle of a drop deposited on the sample surface remained unchanged over time, in the case of CT, the contact angle dropped to ~0° after half a minute (Fig. 4d), implying that the hydrophobic effect is less marked in the latter case. These results are consistent with the observed water absorption coefficients for these samples, as the contact angle is a critical parameter determining water sorptivity (i.e., the higher the contact angle the lower the sorptivity) [72]. This TEOS-induced hydrophobic effect is known to be transient [12,68]. However, we measured the contact angle after immersion in water for 7 days, and the values we obtained were almost unchanged (78.9° and 43.9° for T and CT, respectively). This shows that the hydrophobic effect of TEOS-based treatments can be relatively long-lasting. Franzoni et al. [70] report that even after 7-month curing, TEOS still shows the presence of Si-O-C bonds (detected by FTIR) of non-hydrolyzed ethoxy groups, which impart hydrophobicity. This is evidence of a very slow curing for this type of treatment, which may jeopardize its consolidation capacity, especially at an early age. The fact that the contact angle is lower in the case of CT could indicate that the hydrolysis of the TEOS component is accelerated in the presence of $Ca(OH)_2$.

Finally, we measured the water vapor transmission (WVT) of untreated and treated samples (Fig. 4e). As expected, a reduction in WVT rates (WVTR) was detected after the treatments. WVTR values for the different samples were 7.78×10^{-7}, 6.94×10^{-7}, 6.39×10^{-7}, 6.67×10^{-7}, and 5.83×10^{-7} g cm^{-2} s^{-1} for CO, W, C, T, and CT, respectively. Reductions in WVTR of 8%, 4%, and 16% as compared with the W control were observed for the C, T, and CT treatments, respectively, which are below the maximum acceptable reduction (≤20%) for consolidation treatments [2]. These results are consistent with the observed reduction in porosity (i.e., results of MIP and water absorption under vacuum) associated with the deposition of the consolidants in the pore system of the stone. Yet, paths for water vapor flow through the stone were present after treatment, ensuring that despite the observed reduction in WVTR, the samples were sufficiently permeable for water vapor. This is a critical issue for any consolidation treatment [1,2], as an excessive reduction in WVTR is highly deleterious, especially in the case of salt damage, thermal shock and/or frost damage situations [5].

3.6. *Textural and microstructural features*

FESEM-EDS analysis shows that CO samples display standard textural features of a biocalcarenite, that is, a clastic sedimentary rock (Fig. 5a). The microstructure was highly porous and grain supported, with angular grains of quartz, feldspars and calcite, cemented by microsparitic calcite and clay minerals. Note that due to their small amounts, the clay minerals were not detected by XRD. The largest calcite grains are bioclasts including mollusk shells and coccoliths. Following the salt weathering test, cement around quartz, feldspars and calcite/bioclast grains was partially lost, resulting in a porosity increase.

Samples treated with C showed intergranular deposits of newly formed nanogranular calcium carbonate (calcite) generated by the reaction of nanolime with carbon dioxide (Fig. 5b). Compared with the control samples, the surface structure of the treated stone was denser and nanolime-derived calcite cement accumulated in pores and valleys, an effect which would contribute to the strengthening of the stone, yet this effect was limited to the surface and near-surface of the samples.

In T-treated samples, the gel formed after the reaction of TEOS and the biocalcarenite substrate filled the intergranular pores of the weathered stone creating a thick surface film that blanketed all grains and pores (Fig. 5c). Compared with C samples, the porosity reduction was more obvious, and the reduction of macropores was particularly marked. We also observed pervasive cracking of the silica gel film, which as indicated above is one of the main drawbacks of this type of treatment [7].

In CT samples, the consolidant filled the intergranular pores of the stone (Fig. 5d). The consolidant cement displayed a gel-like structure, and in some areas, drying cracks were observed. Apparently, in the case of T and CT treatments, such drying cracks did not appear to negatively affect their consolidation capacity, as shown by the above-described test results demonstrating a significant strengthening effect in both cases. However, we will see below that the more abundant cracks in T as compared with CT (and the lack of bonding with the carbonate grains of the former) jeopardize the durability of the T treatment.

3.7. Drilling resistance of treated stones subjected to salt weathering test

To evaluate the long-term performance of T and CT treatments, treated samples were subjected to the salt weathering test (i.e., 15 cycles, EN 12370) and their durability was assessed by DR. Only samples treated with T and CT were considered as only those showed a significant degree of consolidation in terms of physical-mechanical properties and porosity reduction.

Fig. 6 shows the DR plots for samples treated with T and CT prior to and after the salt weathering test (with CO as reference). Despite the relatively high standard deviation, there was a clear reduction in DR values of samples treated with T and subjected to weathering, with DR values approaching those of the control. In contrast, samples treated with CT showed no detectable reduction in DR values along the depth profile after salt weathering as compared with unweathered samples. Actually, there was a slight increase in DR after weathering all along the depth profile, which could be due to an increased level of hydrolysis and polycondensation as these samples were tested after 4 months from treatment application and were in contact with an aqueous saline solution [70]; yet this increase was within error. It follows that the CT treatment presents higher durability than the T treatment when subjected to accelerated weathering, which proves its superior long-term consolidation effectiveness. It is very likely that the reduced drying cracks density, as well as the possible strong bonding between the consolidant and the carbonate substrate brought about by the formation of C-S-H in CT (see the following section), are key to explaining such an excellent performance upon weathering.

3.8. Reaction of TEOS and $Ca(OH)_2$ nanoparticles

To identify possible reaction mechanisms and products of the alkoxysilane-$Ca(OH)_2$ nanoparticle mixture, we cured the consolidants (T and CT with 1:3 vol ratio) in petri dishes under laboratory conditions. The resulting gels were aged for one month, and samples were collected and ground prior to analysis. Fig. 7a and 7b show the FTIR spectra of the reference T and CT, respectively. In both cases the following bands were identified: the Si-O-Si asymmetric and symmetric stretching at 1036–1042 and 787–788 cm^{-1}, respectively, the shoulder at 1154–1160 cm^{-1} corresponding to LO_4 vibrations, the Si-O stretching of silanol (Si-OH) and Si-O groups at 951–968 cm^{-1}, and the strong band at 410–411 cm^{-1} corresponding to SiO_4 tetrahedra. These bands are standard for amorphous silica gel [26,73,74,75,76], but are also present in C-S-H, although with different intensities: i.e., the most intense band of C-S-H is the Si-O at 970 cm^{-1}, corresponding to Q^2 tetrahedra [77,78,79]. Because the bands overlap, it is difficult to single out the contribution of silica gel and C-S-H in the CT spectrum. However, the more marked shoulder at 1194 cm^{-1} corresponding to TO_4 (i.e., Q^4 units in highly polymerized silica gel) and the broad band at 559 cm^{-1} corresponding to the siloxane backbone/silicate rings in silica gel, were not well-defined in CT sample. Conversely, a blue shift and broadening of

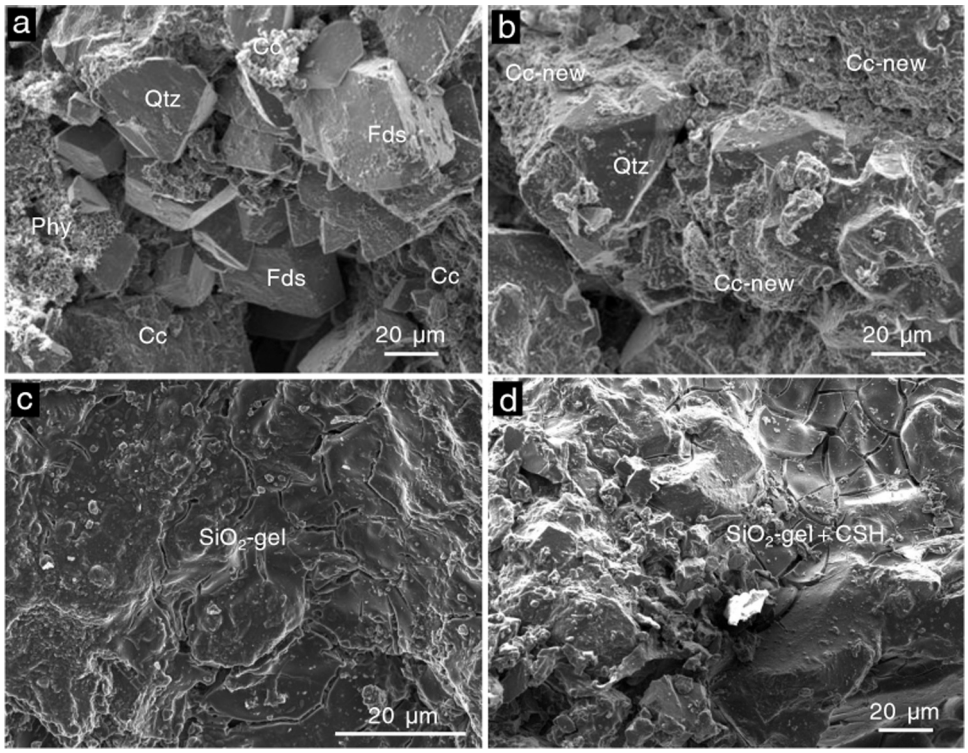

Fig. 5. FESEM images of samples before and after consolidation. a) CO sample; b) C sample; c) T sample. Note pervasive drying cracks all over the surface; d) CT sample. Note drying cracks in some areas (upper right). Legend: Qtz, quartz; Fds, feldspar; Cc, calcite; Phy, phyllosilicates; Cc-new, calcite formed after $Ca(OH)_2$ carbonation; SiO_2-gel, silica gel formed after TEOS; SiO_2-gel+CSH, gel including silica and C-S-H formed after CT.

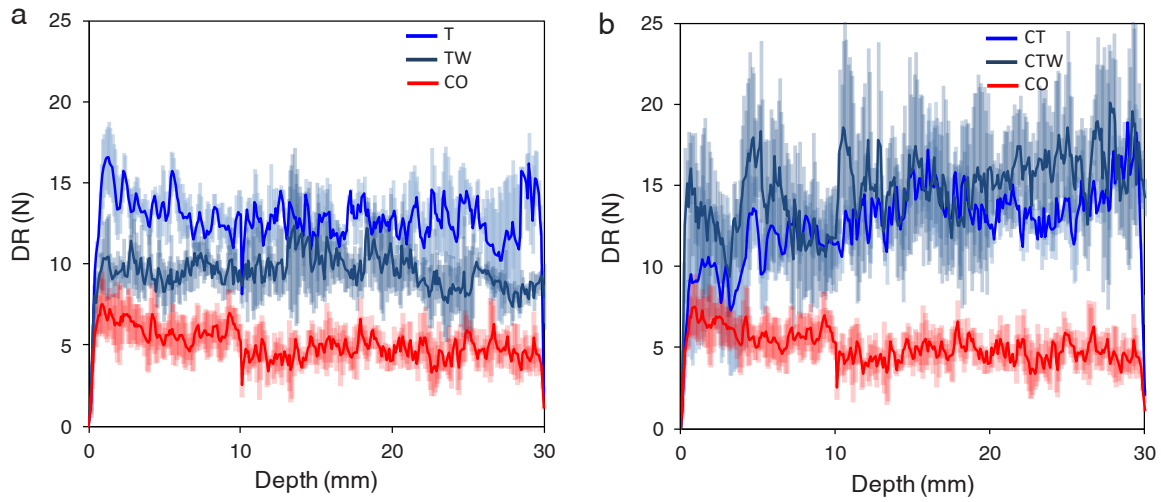

Fig. 6. Drilling resistance (DR) of untreated (CO), treated (T and CT) and treated+weathered (TW and CTW) stone samples: a) T treatment; b) CT treatment.

the Si-O band from 951 cm^{-1} in silica gel to 968 cm^{-1} in CT occurred, and additional small bands (585–664 cm^{-1}) exclusive of C-S-H were observed in CT but not in the silica gel formed after TEOS. These results suggest that C-S-H (along with silica gel) formed in the case of CT. However, the most compelling evidence for the formation of C-S-H in CT samples is the fact that neither the OH stretching band at 3640 cm^{-1} of $Ca(OH)_2$ (i.e., unreacted nanolime), nor the strong carbonate bands at ~1400 cm^{-1}, corresponding to $CaCO_3$ product of nanolime carbonation, were detected. This means that all calcium in the nanolime reacted with TEOS (at highly alkaline conditions) to yield a new phase, i.e., C-S-H. Considering that the Ca/Si mole fraction in CT is 0.04, this means that full consumption of $Ca(OH)_2$ will lead to 4 mol% C-S-H (and 96 mol% silica gel) in the final CT product (assuming a Ca/Si mole ratio of 1 in standard C-S-H). Note that a classical route for the production of C-S-H is

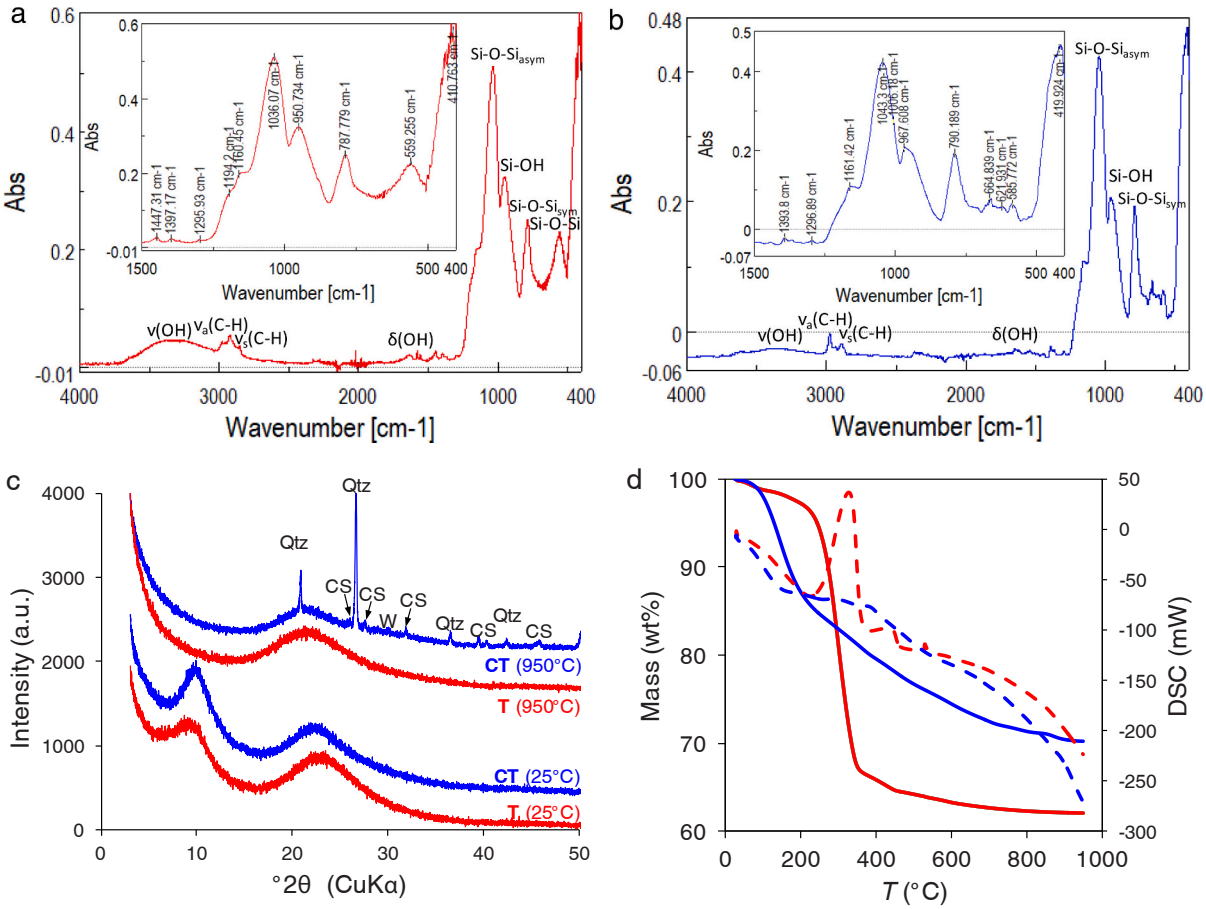

Fig. 7. Characterization of TEOS and the reaction product of TEOS and nanolime mixtures. FTIR spectra of (a) T and (b) CT products. Insets show an enlarged section of the spectra; (c) XRD patterns of T and CT before and after thermal treatment (2 h at 950 °C). Legend: Qtz, quartz, CS, calcium silicate ($CaSiO_3$); W, β-wollastonite; (d) TG-DSC of pure TEOS product (blue curves) and CT product (red curves). Solid curves: TG traces; dashed curves: DSC traces.

the reaction in solution of CaO/$Ca(OH)_2$ with amorphous or soluble silica [80,81]. Moreover, it is known that the application of TEOS on hardened cement consumes $Ca(OH)_2$ (a major phase in Portland cement) leading to the formation of C-S-H [27,82], as also does the reaction of TEOS with $Ca(OH)_2$ solutions [83,84], nanolimes [25], and $Ca(OH)_2$ pastes [26]. Finally, the C-H stretching bands of CH_2 and CH_3 groups at 2800–2900 cm^{-1} were still present in both T and CT products, showing that the hydrolysis reaction of ethoxy groups was not complete (after one month) and/or some ethanol got trapped/adsorbed within the gel matrix [26].

XRD analyses showed that both T and CT products are amorphous (Fig. 7c). This is consistent with the formation of silica gel in both cases, as well as additional amorphous C-S-H in the latter case. The fact that we observe no Bragg peaks of portlandite or any $CaCO_3$ polymorphs agrees with the FTIR results and confirms that all calcium in the nanolime has been consumed to form a new amorphous phase (i.e., C-S-H). Interestingly, the XRD pattern of both T and CT products showed the standard hump at ~20–30 °2θ of silica gel [11], plus an additional hump at a lower angle (~7–12 °2θ). Note that metal alkoxides (e.g., calcium alkoxides) typically have a planar structure (CdI_2-type core geometry) with basal d_{001}-spacing of ~8–10 Å, corresponding to ~9–11 °2θ [64,85]. It is thus likely that this low-angle hump corresponds to a poorly crystalline or nearly amorphous (but with a defined short-range order) precursor silicon alkoxide. This is consistent with the fact that full hydrolysis was not achieved after one month of curing. To further disclose whether C-S-H formed in CT upon curing, both T and CT solids were heated at 950 °C for 2 h in an electric furnace (air-ventilated) and subsequently analyzed by XRD [11]. As expected, no crystalline phase formed in the case of thermally treated T. Conversely, quartz plus two calcium silicate phases (β-wollastonite, ICDD card # 84–654 and unnamed $CaSiO_3$, ICDD card # 89–6463) formed in the case of thermally treated CT (Fig. 7c). The formation of crystalline calcium silicate phases upon thermal treatment of C-S-H has been reported [11,86], demonstrating that such an amorphous C-S-H phase was indeed present in the CT solid product. The formation of quartz in the case of CT is likely due to the fluxing effect of the calcium phases present, enabling partial melting of the mixture followed by crystallization of quartz. Interestingly, both thermally treated T and CT samples no longer show the hump at 7–12 °2θ, which is consistent with the thermal decomposition of the alkoxide precursor (see TG-DSC results below).

TG-DSC analyses of T and CT products provided further evidence for the formation of C-S-H after CT curing (Fig. 7d). TEOS-derived solids showed a first mass loss of 3 wt% at 25–203 °C, a second of 29 wt% at 203–350 °C, and a third of 5 wt% at 350–600 °C. According to Zarzuela et al. [26], the first two correspond to the evaporation of reaction byproducts (H_2O and EtOH) physisorbed on the surface or trapped in the gel pores, and the last one to oxidative decomposition (combustion) of non-hydrolyzed ethoxy groups from precursor TEOS. While the first weight loss corresponds to an endothermic band, consistent with an evaporation event, the last two weight losses are associated with two marked exothermic peaks. The higher T exothermic peak is consistent with a combustion process (thermal decomposition of ethoxy groups), as indicated by Zarzuela et al. [26]. However, the first and most intense exothermic peak is not consistent with the evaporation/desorption event proposed by Zarzuela et al. [26], which should be endothermic. It is more likely that the main exothermic peak in TEOS-derived dried gels at 275–400 °C is due to the combustion of organic carbon (ethanol) as indicated by Brinker et al. [87]. Conversely, the dry product of CT sol-gel transition shows a nearly continuous weight loss from room T up to 900 °C, with a total weight loss lower than that of the TEOS product (30 vs 38 wt%). This is consistent with the presence of C-S-H along with silica gel. Garbev et al. [86] reported that after an initial weight loss due to vaporization of adsorbed water at $T < 200$ °C, C-S-H shows a nearly continuous, monotonically decreasing weight loss associated with loss of structural water and dehydroxylation of silanol groups (at the highest T) resulting in the final formation of β-wollastonite, as observed here. We also observed a small and broad exothermic band at 260–450 °C due to the combustion of carbon, reflecting the presence of adsorbed/trapped ethanol, and unhydrolyzed ethoxy groups.

Further conclusive evidence for the formation of C-S-H (along with silica gel) was provided by TEM-EDS analysis of the CT product (Fig. 8). We observed gel-like aggregates made up of fibrous- and/or lath-like and granular nanosized precipitates, which were amorphous as shown by the diffuse rings in their SAED pattern (Fig. 8a-c). HAADF imaging and corresponding EDS elemental analysis showed that such precipitates include Ca and Si, along with O (Fig. 8d). Point EDS analysis revealed that some of the amorphous aggregates were Si-rich (nanogranular precipitates) whereas others included similar contents of Ca and Si (fibrous- or lath-like precipitates) (Fig. S6), consistent with the presence of amorphous silica and Type-I C-S-H (which typically displays a fibrous/lath-like habit) [88,89].

Altogether, these spectroscopic, textural/structural, and compositional results confirm the formation of both silica gel and C-S-H as the cementing end-products of our CT consolidant.

It has been proposed that the reaction of TEOS and $Ca(OH)_2$ (the latter dosed as solid or as a saturated solution) resulting in the formation of C-S-H is a pozzolanic reaction [11,25,83,84]. Eqs. (3) and (4) present a plausible overall two-step mechanism for the pozzolanic reaction between $Ca(OH)_2$ and silica (gel) formed after TEOS [25,82,90]:

$$Si(OC_2H_5)_4 + 2H_2O \rightarrow SiO_2 + 4C_2H_5OH \quad (3)$$

$$nCa(OH)_2 + SiO_2 + mH_2O \rightarrow nCaO\bullet SiO_2\bullet(n+m)H_2O \quad (4)$$

.

However, this set of reactions, which could play a role in the case of nanosilica or TEOS applied to set cement (where portlandite is already present) [11,82], seems to be an oversimplification in the case of the reaction of TEOS and nanolime in our studied CT system. The above mechanistic model implies that the pozzolanic reaction (Eq. 4) would take place upon completion of TEOS hydrolysis and polycondensation resulting in the formation of silica gel. Then, the alkaline dissolution of silica gel would result in the precipitation of C-S-H. But TEOS sol-gel reactions are very slow (several days to weeks, or even months) [7,15,70,84]. This would enable the $Ca(OH)_2$ nanoparticles in CT to react with atmospheric CO_2 and fully carbonate, as they do so in a few days [63]. The latter would prevent the development of any pozzolanic reaction. However, we observed no carbonate phases forming upon curing of CT. It is thus much more likely that Ca^{2+} ions from $Ca(OH)_2$ dissolution (enabled by humidity) directly reacted with the product of the alkaline (catalyzed) hydrolysis of TEOS (taking place in the presence of H_2O, plus OH^- supplied by the dissolution of nanolime particles). This way, silanol groups (Si-OH) would directly react with calcium ions forming Si-O-Ca bonds, thus enabling the formation of the C-S-H phase. This agrees with previous research which proposes direct alkaline cleavage of oligomeric TEOS and direct bonding of reactive silanol with Ca^{2+} from portlandite to form C-S-H [26,91]. The proton released upon silanol cleavage would in turn react with a hydroxyl group forming a water molecule. The H_2O product would further contribute to the progress of (alkaline) TEOS hydrolysis and the formation of C-S-H. In this case, the assumed pozzolanic reaction between TEOS and $Ca(OH)_2$ (nano)particles [11,25,84], will not be at work. Considering that (reactive) silica dissolution is the rate-determining step of a pozzolanic reaction, bypassing this step by the direct reaction of hydrolyzed TEOS with calcium ions at highly alkaline pH, speeds up the formation of C-S-H [83], which is relevant for an effective consolidation treatment.

3.9. Implications of C-S-H formation upon CT treatment

The fact that the treatment with CT results in the formation of C-S-H (along with silica gel) has important implications. It explains the superior performance and durability in terms of strength improvement with no negative side effects of CT in the case of biocalcarenite stone. First, C-

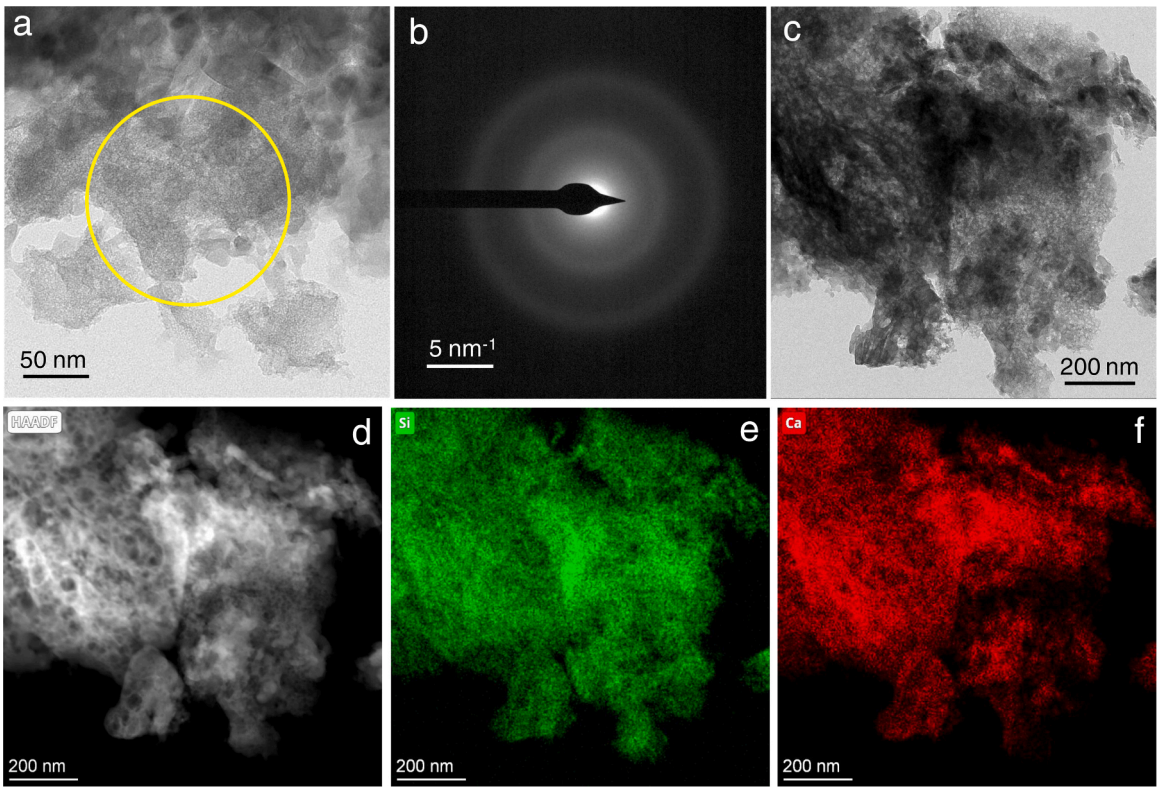

Fig. 8. TEM analysis of CT products. a) Bright field image of porous fibrous and lath-like aggregates; b) SAED pattern of the yellow circled area in (a) showing diffuse rings indicative of an amorphous phase; c) Bright filed image of an aggregate of amorphous gel made up of fibrous and lath-like precipitates; d) HAADF image of the area shown in (c). Note the porous nature of the gel (most visible on the left); EDS Si map (e) and Ca map (f) of the area in (d).

S-H formation as fibrous or lath-like nanoparticles can help limit drying shrinkage of the silica gel and the associated cracking, in a similar fashion as the addition of a range of nanoparticles (e.g., SiO_2, TiO_2) to TEOS [16,92]. As a result, the loss of cohesion and cementing capacity of silica gel is minimized. However, it is not fully prevented, as we observed some drying cracks in cured CT products and the CT-treated stones. Further research should focus on the reduction of drying crack development upon CT curing, for instance using surface active agents [10] and/or additional nanoparticles (i.e., either inert SiO_2 or photo-active TiO_2 or ZnO) [92]. Second, in contrast to silica gel that does not establish bonds with carbonate substrates [7], C-S-H has a strong bonding capacity with carbonate substrates (e.g., limestone aggregate), even stronger than that achieved with silicate substrates (e.g., siliceous aggregate) [93]. As indicated by Ouyang et al. [93], this is due to the capacity of $CaCO_3$ substrates to strongly bond Ca^{2+} ions, which can, in turn, bond via strong covalent bonding to the tobermorite-like lamellae of C-S-H. This is consistent with the observation that C-S-H heterogeneously nucleates on calcite [94], demonstrating the chemo-structural affinity between the two phases. It follows that C-S-H does not only act as a coupling agent between silica gel and the carbonate substrate as previously assumed [22], but rather by establishing such strong bonding that directly contributes to the observed strengthening and long-lasting performance upon application to the biocalcarenite stone. Third, despite the assumed catalytic action that a strong base such as $Ca(OH)_2$ should have on the hydrolysis and polycondensation of TEOS, viscosity does not seem to be significantly altered, enabling deep penetration of the CT consolidant. This could be due to the fact that upon hydrolysis of TEOS, Ca^{2+} ions hamper silica gel polycondensation by bonding siloxane units and forming discrete nanoparticles of C-S-H, thus delaying viscosity increase and densification during the sol-gel transition. We have to also note that the 1:3 mixture in the CT consolidant results in a 25% dilution of the TEOS component, which could also favor penetration. Altogether, these effects help explaining the MIP and DR results showing accumulation of the CT consolidant in depth, leading to increased DR, an effect that to our knowledge has never been reported for TEOS. Yet further research on the kinetics of hydrolysis/polycondensation of TEOS-nanolime mixtures and their rheology evolution is necessary to validate the above hypothesis. Fourth, it is important to note that the CT treatment maintained its effectiveness in terms of DR even after 15 salt weathering cycles and outperformed the T treatment, which failed to provide satisfactory long-term durability. Fifth, as compared with nanolime, the newly formed C-S-H cement is stronger than $CaCO_3$ cement formed after carbonation of nanolime wihout the risk of back migration as often observed in the case of nanolime. As a result, an effective in-depth consolidation is achieved with the CT treatment, whereas the nanolime treatment only results in a very limited surface consolidation. However, we must note that in our tests only one complete nanolime treatment (until saturation) was applied. It is likely that better performance would be achieved if the nanolime treatment were applied several times [65]. Sixth, because the release of ethanol after CT curing (as occurs with TEOS) is very slow, the treatment retains surface-adsorbed ethoxy/ethyl groups for a long time, which imparts a certain degree of hydrophobicity (as shown by the contact angle measurements and the water absorption behavior), leading to a transient protective effect. Yet the treatment neither blocks/plugs the pores nor reduces significantly the water vapor transmission, and achieves optimal strengthening.

Finally, we want to stress the fact that in our selected 1:3 nanolime: TEOS mixture, the Ca/Si mole ratio was very low (0.04), which ensured that there was an excess of Si to combine with Ca to form C-S-H. Such an excess of Si explains why all Ca available was consumed in the formation of C-S-H, not just in the case of the 1:3 formulation, but also in all preliminary tested mixes, from 1:4 up to 4:1 vol:vol C:T, as shown by our FTIR analyses (Fig. 7b; Fig. S2c). Note, however, that there is room to increase the Ca content in the mixtures (by adding more concentrated nanolime dispersions to TEOS) as to increase the amount of C-S-H

formed upon reaction, an aspect that can be exploited for producing thicker and stronger cementing formulations for a range of applications (e.g., putties or injection grouts for re-aggregation and filling fractures, or pure calcium silicate cements). In any case, here we demonstrate that the formation of just 4 mol% C-S-H in silica gel after CT curing, is enough to bright about the beneficial effects above described when this treatment is applied on porous calcareous stone, with no side effects indicative of incompatibility issues.

4. Conclusions

Our results show that the combination of nanolime and TEOS in a 1:3 vol ratio results in a promising strategy for the consolidation of carbonate stones that overcomes the main limitations of both individual consolidants, while showing no detrimental side effects. The improvements achieved by our CT treatment are manifold. The CT treatment results in negligible changes in stone appearance, provoking the lowest color change of all consolidation treatments. Based on porosity and DR results, comparable or even higher penetration than TEOS is achieved, while avoiding the risk of back migration as observed for nanolime. Furthermore, CT was not only most effective in reestablishing surface cohesion and improving surface hardness, as revealed by the peeling and HLD tests, but also resulted in higher mechanical strength of the stone as demonstrated by the *Vp*, tensile strength, and DR results. None of the treatments under study here had any negative effect on the water behavior (absorption and drying) and water vapor permeability of the treated stone. Nonetheless, the TEOS-based treatments (T and CT) impart a certain (transient) hydrophobicity due to the incomplete hydrolysis of ethoxy groups, without, however, jeopardizing treatment performance. Importantly and in stark contrast to TEOS-treated biocalcarenite, the CT-consolidated stone does not suffer any reduction in DR along the depth profile after the accelerated ageing test, proving its long-term durability.

Our results show that the optimal consolidation efficacy and durability achieved by the CT treatment applied to a porous calcareous stone is due to the formation of a C-S-H gel. The evidence for the formation of C–S–H upon interaction of nanolime and TEOS in the CT treatment is multiple, as shown by the FTIR, XRD, TG-DSC and TEM-EDS analyses of CT product after curing and thermal treatment. C-S-H formation occurs by direct reaction between Ca^{2+} ions and Si-OH groups, resulting in Si-O-Ca bond formation, and not involving a pozzolanic reaction between $Ca(OH)_2$ and silica gel, as commonly assumed. For this reaction to take place at an optimal rate and yield, the high surface area to volume ratio of nanolime is of outmost importance, ensuring high reactivity and fast dissolution to provide adequate release of Ca^{2+} and OH^- ions for C-S-H formation. The formation of C-S-H in CT reduces drying cracks development and enables strong bonding between the cementing product (amorphous silica gel plus the C-S-H gel) and the carbonate substrate. Importantly, the presence of Ca^{2+} ions is not only crucial for the formation of C-S-H, but also to prevent early polymerization, thereby delaying the increase in viscosity associated with the sol-gel transition. The latter explains why the CT treatment has a better penetration than TEOS.

Altogether, our results demonstrate that the combination of nanolime and TEOS is a highly promising strategy for the design and application of more effective consolidants for calcareous stones and, potentially, other calcareous building materials. Further research should be performed to evaluate other possible mixing ratios of these two products for different applications. The fact that drying cracks still form in the case of CT-cured products makes it necessary to explore possible formulations aimed at reducing such an effect, for instance using surfactants and/or additional nanoparticles. Finally, (small scale) field tests should be performed to further gauge the effectiveness of CT treatments for the consolidation of calcareous stones.

CRediT authorship contribution statement

Elert Kerstin: Writing – review & editing, Validation, Methodology, Investigation, Conceptualization. **Rodriguez-Navarro Carlos:** Writing – original draft, Validation, Supervision, Project administration, Methodology, Investigation, Funding acquisition, Conceptualization. **He Jing:** Writing – review & editing, Validation, Methodology, Investigation. **Crespo-López Laura:** Writing – review & editing, Investigation. **Otero Jorge:** Writing – original draft, Validation, Supervision, Methodology, Investigation, Conceptualization. **Benavides-Reyes Cristina:** Writing – review & editing, Investigation. **Monasterio-Guillot Luis:** Writing – review & editing, Investigation.

Declaration of Competing Interest

The authors declare that they have no known competing financial interests or personal relationships that could have appeared to influence the work reported in this paper.

Data availability

Data will be made available on request.

Acknowledgements

We acknowledge funding by the Spanish Government grant PID2021–125305NB-I00 funded by MCIN/ AEI /10.13039/501100011033 and by ERDF A way of making Europe, Junta de Andalucía research group RNM-179 and grant P20_00675, University of Granada, Unidad Científica de Excelencia UCE-PP2016–05, Funding for open access charge: Universidad de Granada/CBUA. J.O. research is funded by the European Commission on the Marie Skłodowska-Curie Actions (MSCA-IF) from the European Union's Horizon 2020 on Research and Innovation, grant agreement no. 893762 (NANOMORT).

Appendix A. Supporting information

Supplementary data associated with this article can be found in the online version at doi:10.1016/j.conbuildmat.2024.135437.

References

[1] E. Doehne, C.C. Price, Stone Conservation: An Overview of Current Research, Getty Conservation Institute, Los Angeles, 2010.
[2] S. Siegesmund, R. Snethlage (Eds.), Stone in Architecture: Properties, Durability, 5th edition, Springer-Verlag, Berlin, 2014.
[3] J. Delgado Rodrigues, Consolidation of Decayed Stones. A Delicate Problem with Few Practical Solutions. in International Seminar on Historical Constructions. 3-14. Guimarães, Portugal (2001).
[4] Y. Praticò, F. Caruso, J. Delgado Rodrigues, F. Girardet, E. Sassoni, G.W. Scherer, V. Vergès Belmin, N.R. Weiss, G. Wheeler, R.J. Flatt, Stone consolidation: a critical discussion of theoretical insights and field practice, RILEM Tech. Lett. 4 (2020) 145–153.
[5] J.R. Clifton. Stone Consolidating Materials: A Status Report (Vol. 1118), Department of Commerce, National Bureau of Standards, Washington, 1980.
[6] H.R. Sasse, R. Snethlage, Methods for the Evaluation of Stone Conservation Treatments, in: N.S. Baer, R. Snethlage (Eds.), Saving our Architectural Heritage: the Conservation of Historic Stone Structures, John Wiley & Sons, New York, 1997, pp. 223–243.
[7] G. Wheeler, Alkoxysilanes and the Consolidation of Stone, Getty Publications, Los Angeles, 2005.
[8] M. Laurenzi-Tabasso, S. Simon, Testing methods and criteria for the selection/evaluation of products for the conservation of porous building materials, Rev. Conserv. 7 (2006) 67–82.
[9] J. Delgado Rodrigues, A. Grossi, Indicators and ratings for the compatibility assessment of conservation actions, J. Cultur. Herit. 8 (2007) 32–43.
[10] M.J. Mosquera, D.M. de los Santos, A. Montes, L. Valdez-Castro, New nanomaterials for consolidating stone, Langmuir 24 (2008) 2772–2778.
[11] F. Sandrolini, E. Franzoni, B. Pigino, Ethyl silicate for surface treatment of concrete–Part I: Pozzolanic effect of ethyl silicate, Cem. Concr. Comp. 34 (2012) 306–312.
[12] E. Franzoni, G. Graziani, E. Sassoni, G. Bacilieri, M. Griffa, P. Lura, Solvent-based ethyl silicate for stone consolidation: influence of the application technique on

penetration depth, efficacy and pore occlusion, Mater. Struct. 48 (2015) 3503–3515.
[13] F. Xu, W. Zeng, D. Li, Recent advance in alkoxysilane-based consolidants for stone, Prog. Org. Coat. 127 (2019) 45–54.
[14] C. Pötzl, S. Rucker, E. Wendler, S. Siegesmund, Consolidation of volcanic tuffs with TEOS and TMOS: a systematic study, Environ. Earth Sci. 81 (2022) 1–27.
[15] C.J. Brinker, G.W. Scherer, Sol-Gel Science: the Physics and Chemistry of Sol-gel Processing, Academic press, New York, 1990.
[16] C. Miliani, M.L. Velo-Simpson, G.W. Scherer, Particle-modified consolidants: a study on the effect of particles on sol–gel properties and consolidation effectiveness, J. Cult. Herit 8 (2007) 1–6.
[17] G.W. Scherer, G. Wheeler, Silicate consolidation for stone, Key Eng. Mater. 391 (2009) 1–25.
[18] P. Maravelaki-Kalaitzaki, N. Kallithrakas-Kontos, Z. Agioutantis, S. Maurigiannakis, D. Korakaki, A comparative study of porous limestones treated with silicon-based strengthening agents, Prog. Org. Coat. 62 (2008) 49–60.
[19] A. Burgos-Cara, C. Rodríguez-Navarro, M. Ortega-Huertas, E. Ruiz-Agudo, Bioinspired alkoxysilane conservation treatments for building materials based on amorphous calcium carbonate and oxalate nanoparticles, ACS Appl. Nano Mater. 2 (2019) 4954–4967.
[20] N.R. Weiss, I. Slavid, G. Wheeler, Development and Assessment of A Conversion Treatment for Calcareous Stone, in: V. Fassina (Ed.), Proc. 9th International Congress on Deterioration and Conservation of Stone, 2, Elsevier, Amsterdam, 2000, pp. 533–540.
[21] Slavid, I.O., Weiss, N.R., Method for Protecting and Consolidating Calcareous Materials. US patent 6296905. 2 October (2001).
[22] G. Ziegenbalg, M. Drdácký, C. Dietze, D. Schuch, Nanomaterials in Architecture and Art Conservation, CRC Press, 2018.
[23] E. Maryniak-Piaszczynski, V. Wolf, E. Ghaffari, The Combination of Calcium Hydroxide-sol and Silicic Acid Ester as New Method for the Structural Consolidation of Objects Built of Tuff, Lime Marl, Trachyte–latest Findings. In Proc. 12th International Congress on the Deterioration and Conservation of Stone, New York (2012), pp. 1-12.
[24] P. D'Armada, E. Hirst, Nano-lime for consolidation of plaster and stone, J. Architect Conserv. 18 (2012) 63–80.
[25] A.M. Barberena-Fernández, M.T. Blanco-Varela, P.M. Carmona-Quiroga, Use of nanosilica-or nanolime-additioned TEOS to consolidate cementitious materials in heritage structures: Physical and mechanical properties of mortars, Cem. Concr. Comp. 95 (2019) 271–276.
[26] R. Zarzuela, M. Luna, L.M. Carrascosa, M.P. Yeste, I. Garcia-Lodeiro, M.T. Blanco-Varela, M.A. Cauqui, J.M. Rodríguez-Izquierdo, M.J. Mosquera, Producing C.S.H. gel by reaction between silica oligomers and portlandite: a promising approach to repair cementitious materials, Cem. Concr. Res. 130 (2020) 106008.
[27] I. Garcia-Lodeiro, R. Zarzuela, M.J. Mosquera, M.T. Blanco-Varela, Consolidation of artificial decayed portland cement mortars with an alkoxysilane-based impregnation treatment and its influence on mineralogy and pore structure, Constr. Build. Mater. 304 (2021) 124532.
[28] G. Borsoi, M. Tavares, R. Veiga, A.S. Silva, Microstructural characterization of consolidant products for historical renders: an innovative nanostructured lime dispersion and a more traditional ethyl silicate limewater solution, Microsc. Microanal. 18 (2012) 1181–1189.
[29] M. Matos, G. Borsoi, R. Veiga, P. Faria, A. Santos-Silva, Durability to Marine Environment of Innovative Products for Consolidation and Chromatic Reintegration of Historical Renders. In 9th International Masonry Conference (pp. 1-10; CD-ROM). Universidade do Minho/Instituto para Sustentabilidade em Engenharia Estrutural (ISISE)/International Masonry Society (IMS) Guimaraes (2014).
[30] A. Michalopoulou, P.N. Maravelaki, V. Kilikoglou, I. Karatasios, Morphological characterization of water-based nanolime dispersions, J. Cult. Herit. 46 (2020) 11–20.
[31] V. Barnoos, A. Shekofteh, O. Oudbashi, Experimental evaluation of the consolidation treatments of low porosity limestone from the historic monument of the anahita temple of kangavar, Iran. Archaeol. Anthropol. Sci. 14 (2022) 63.
[32] M.A.B. López, Caracterización y estado de alteración química de los materiales empleados en la construcción de la catedral de sevilla, Ph.D. thesis, Universidad de Sevilla (1988).
[33] C.R. Hubbard, R.L. Snyder, RIR-measurement and use in quantitative XRD, Powd. Diffract. 3 (1988) 74–77.
[34] NORMAL 20/85, Interventi Conservativi: Progettazione Esecuzione E Valutazione Preventiva, Milan, Italy (1996).
[35] EN 12370, Natural Stone Test Methods—determination of Resistance to Salt Crystallization, 1999–2003, CEN (Comité Européen de Normalization), Brussel, Belgium, 1999.
[36] B. Lubelli, V. Cnudde, T. Diaz-Goncalves, E. Franzoni, R.P. van Hees, I. Ioannou, B. Menendez, C. Nunes, H. Siedel, M. Stefanidou, V. Verges-Belmin, H. Viles, Towards a more effective and reliable salt crystallization test for porous building materials: state of the art, Mater. Struct. 51 (1) (2018) 21.
[37] ASTM D-2845-05, Measuring Rocks Geotechnical Properties Using Ultrasonic Waves. American System for Testing and Materials, Philadelphia (2006).
[38] RILEM Commission PEM-25, Protection et Erosion des Monuments Recommended tests to measure the deterioration of stone and to assess the effectiveness of treatment methods. Mater. Struct. 13 (1980) 175-253.
[39] J. Otero, V. Starinieri, A.E. Charola, Nanolime for the consolidation of lime mortars: A comparison of three available products, Constr. Build. Mater. 181 (2018) 394–407.
[40] A.E. Charola, J. Otero, P.T. DePriest, R.J. Koestler, Built Heritage Evaluation: Manual Using Simple Test Methods, Smithsonian Institution Scholarly Press, Washington, 2021, pp. 29–38.
[41] C. Rodriguez-Navarro, A. Suzuki, E. Ruiz-Agudo, Alcohol dispersions of calcium hydroxide nanoparticles for stone conservation, Langmuir 29 (2013) 11457–11470.
[42] ASTM D3359-09, Standard Test Methods for Measuring Adhesion by Tape Test. American System for Testing and Materials, Philadelphia (2010).
[43] M. Drdácký, J. Lesák, S. Rescic, Z. Slížková, P. Tiano, J. Valach, Standardization of peeling tests for assessing the cohesion and consolidation characteristics of historic stone surfaces, Mater. Struct. 45 (2012) 505–520.
[44] H. Aoki, Y. Matsukura, Estimating the unconfined compressive strength of intact rocks from Equotip hardness, Bull. Eng. Geol. Environ. 67 (2008) 23–29.
[45] K.V. Gogolinskii, V.A. Syasko, A.S. Umanskii, A.A. Nikazov, T.I. Bobkova, Mechanical properties measurements with portable hardness testers: advantages, limitations, prospects, J. Phys. Conf. Ser. 1384 (2019) 012012.
[46] EN 1015-11, Methods of Test for Mortar for Masonry—Part 11: Determination of Flexural and Compressive Strength of Hardened Mortar; European Committee for Standardization, Brusseles, Belgium (1999).
[47] M. Pamplona, M. Kocher, R. Snethlage, L. Aires Barros, Drilling resistance: overview and outlook, Zeit. Deuts. Gesell. Geowissen 158 (2007) 665.
[48] D. Costa, Delgado Rodrigues, Consolidation of A Porous Limestone with Nanolime (pp), Columbia University, New York, 2012, pp. 9–20 (pp).
[49] EN 13755, Natural stone test methods-determination of water absorption at atmospheric pressure", European Committee for Standardization, Brusseles, Belgium (2002).
[50] ASTM C67-000, Standard test methods for sampling and testing brick and structural clay tile. masonry test methods and specifications for the building industry ASTM, , 4th Ed. , Philadelphia , 2001.
[51] EN 16322, Conservation of cultural heritage: test methods: determination of drying properties. European Committee for Standardization, Brussels, Belgium (2013).
[52] J. Otero, V. Starinieri, A.E. Charola, Influence of substrate pore structure and nanolime particle size on the effectiveness of nanolime treatments, Constr. Build. Mater. 209 (2019) 701–708.
[53] UNE-EN 828, Adhesivos - Mojabilidad. Determinación por medida del ángulo de contacto y de la tensión superficial crítica de la superficie sólida. Madrid (2013).
[54] T. López-Martínez, J. Otero, Preventing the undesired surface veiling after nanolime treatments on wall paintings: preliminary investigations, Coatings 11 (2021) 1083.
[55] G. Borsoi, B. Lubelli, R. van Hees, R. Veiga, A.S. Silva, Understanding the transport of nanolime consolidants within Maastricht, limestone. J. Cult. Herit. 18 (2016) 242–249.
[56] M. Burgos-Ruiz, K. Elert, E. Ruiz-Agudo, H. Cölfen, C. Rodriguez-Navarro, Silica-functionalized nanolimes for the conservation of stone heritage, Small 19 (2023) 2300596.
[57] E. Franzoni, E. Sassoni, G.W. Scherer, S. Naidu, Artificial weathering of stone by heating, J. Cult. Herit. 14 (2013) e85–e93.
[58] B. Lubelli, R. Van Hees, T. Nijland, J. Bolhuis, A new method for making artificially weathered stone samples for testing of conservation treatments, J. Cult. Herit. 16 (2015) 698–704.
[59] E. Sassoni, G. Graziani, E. Franzoni, G.W. Scherer, New method for controllable accelerated aging of marble: use for testing of consolidants, J. Am. Ceram. Soc. 101 (2018) 4146–4157.
[60] D.M. Smith, G.W. Scherer, J.M. Anderson, Shrinkage during drying of silica gel, J. Non-Cryst. Solids 188 (1995) 191–206.
[61] N. Alderete, Y. Villagrán, A. Mignon, D. Snoeck, N. De Belie, Pore structure description of mortars containing ground granulated blast-furnace slag by mercury intrusion porosimetry and dynamic vapour sorption, Construct. Build. Mater. 145 (2017) 157–165.
[62] N.M. Alderete, A. Mignon, K. Schollbach, Y. Villagrán-Zaccardi, Deformations in cement pastes during capillary imbibition and their relation to water and isopropanol as imbibing liquids, Materials 15 (2021) 36.
[63] C. Rodriguez-Navarro, K. Elert, R. Ševčík, Amorphous and crystalline calcium carbonate phases during carbonation of nanolimes: implications in heritage conservation, CrystEngComm 18 (2016) 6594–6607.
[64] C. Rodriguez-Navarro, I. Vettori, E. Ruiz-Agudo, Kinetics and mechanism of calcium hydroxide conversion into calcium alkoxides: implications in heritage conservation using nanolimes, Langmuir 32 (2016) 5183–5194.
[65] C. Rodriguez-Navarro, E. Ruiz-Agudo, Nanolimes: from synthesis to application, Pure Appl. Chem. 90 (2018) 523–550.
[66] A. Moropoulou, N. Kouloumbi, G. Haralampopoulos, A. Konstanti, P. Michailidis, Criteria and methodology for the evaluation of conservation interventions on treated porous stone susceptible to salt decay, Progr. Org. Coat. 48 (2003) 259–270.
[67] C. Rodriguez-Navarro, E. Doehne, Salt weathering: influence of evaporation rate, supersaturation and crystallization pattern, Earth Surf. Process. Landf. 24 (1999) 191–209.
[68] S. Yu, C.T. Oguchi, Role of pore size distribution in salt uptake, damage, and predicting salt susceptibility of eight types of Japanese building stones, Eng. Geol. 115 (2010) 226–236.
[69] F. Jroundi, M.T. Gonzalez-Muñoz, A. Garcia-Bueno, C. Rodriguez-Navarro, Consolidation of archaeological gypsum plaster by bacterial biomineralization of calcium carbonate, Acta Biomater. 10 (2014) 3844–3854.
[70] E. Franzoni, G. Graziani, E. Sassoni, TEOS-based treatments for stone consolidation: acceleration of hydrolysis–condensation reactions by poulticing, J. Sol-Gel Sci. Technol. 74 (2015) 398–405.

[71] R. Deshpande, D.W. Hua, D.M. Smith, C.J. Brinker, Pore structure evolution in silica gel during aging/drying. III. Effects of surface tension, J. Non-Cryst. Sol. 144 (1992) 32–44.
[72] L. Yang, D. Gao, Y. Zhang, J. Tang, Y. Li, Relationship between sorptivity and capillary coefficient for water absorption of cement-based materials: theory analysis and experiment, R. Soc. Open Sci. 6 (2019) 190112.
[73] R.M. Almeida, C.G. Pantano, Structural investigation of silica gel films by infrared spectroscopy, J. Appl. Phys. 68 (1990) 4225–4232.
[74] H. Yoshino, K. Kamiya, H. Nasu, IR study on the structural evolution of sol-gel derived SiO_2 gels in the early stage of conversion to glasses, J. Non-Cryst. Sol. 126 (1990) 68–78.
[75] M.C. Matos, L.M. Ilharco, R.M. Almeida, The evolution of TEOS to silica gel and glass by vibrational spectroscopy, J. Non-Cryst. Sol. 147 (1992) 232–237.
[76] R.F. Lenza, W.L. Vasconcelos, Preparation of silica by sol-gel method using formamide, Mater. Res. 4 (2001) 189–194.
[77] P. Yu, R.J. Kirkpatrick, B. Poe, P.F. McMillan, X. Cong, Structure of calcium silicate hydrate (C-S-H): Near-, Mid-, and Far-infrared, spectroscopy. J. Am. Ceram. Soc. 82 (1999) 742–748.
[78] L. Fernandez, C. Alonso, A. Hidalgo, C. Andrade, The role of magnesium during the hydration of C_3S and CSH formation. Scanning electron microscopy and mid-infrared studies, Adv. Cem. Res. 17 (2005) 9–21.
[79] J. Higl, D. Hinder, C. Rathgeber, B. Ramming, M. Lindén, Detailed in situ ATR-FTIR spectroscopy study of the early stages of CSH formation during hydration of monoclinic C_3S, Cem. Concr. Res. 142 (2021) 106367.
[80] H. Le Chatelier, Recherches expérimentales sur la constitution des mortiers hydauliques, Ann. Mines 11 (1887) 345–465.
[81] M. Atkins, F.P. Glasser, A. Kindness, Cement hydrate phase: solubility at 25°C, Cem. Concr. Res. 22 (1992) 241–246.
[82] P. Hou, R. Zhang, Y. Cai, X. Cheng, S.P. Shah, In situ $Ca(OH)_2$ consumption of TEOS on the surface of hardened cement-based materials and its improving effects on the Ca-leaching and sulfate-attack resistivity, Constr. Build. Mater. 113 (2016) 890–896.
[83] A. Moropoulou, A. Cakmak, K.C. Labropoulos, R. Van Grieken, K. Torfs, Accelerated microstructural evolution of a calcium-silicate-hydrate (CSH) phase in pozzolanic pastes using fine siliceous sources: comparison with historic pozzolanic mortars, Cem. Concr. Res. 34 (2004) 1–6.
[84] A.M. Barberena-Fernández, P.M. Carmona-Quiroga, M.T. Blanco-Varela, Interaction of TEOS with cementitious materials: chemical and physical effects, Cem. Concr. Comp. 55 (2015) 145–152.
[85] S.C. Goel, M.A. Matchett, M.Y. Chiang, W.E. Buhro, A very large calcium dialkoxide molecular aggregate having a CdI_2 core geometry: $Ca_9(OCH_2CH_2OMe)_{18}(HOCH_2CH_2OMe)_2$, J. Am. Chem. Soc. 113 (1991) 1844–1845.
[86] K. Garbev, M. Bornefeld, G. Beuchle, P. Stemmermann, Cell dimensions and composition of nanocrystalline calcium silicate hydrate solid solutions. Part 2: X-ray and thermogravimetry study, J. Am. Ceram. Soc. 91 (2008) 3015–3023.
[87] C.J. Brinker, K.D. Keefer, D.W. Schaefer, C.S. Ashley, Sol-gel transition in simple silicates, J. Non-Cryst. Solids 48 (1982) 47–64.
[88] I.G. Richardson, The nature of CSH in hardened cements, Cem. Concr. Res. 29 (1999) 1131–1147.
[89] Z. Zhang, G.W. Scherer, A. Bauer, Morphology of cementitious material during early hydration, Cem. Concr. Res. 107 (2018) 85–100.
[90] H.F. Taylor. Cement Chemistry, Thomas Telford, London, 1997.
[91] I. Garcia-Lodeiro, P.M. Carmona-Quiroga, R. Zarzuela, M.J. Mosquera, M. T. Blanco-Varela, Chemistry of the interaction between an alkoxysilane-based impregnation treatment and cementitious phases, Cem. Concr. Res. 142 (2021) 106351.
[92] M.R. Escalante, G.W. Scherer, J. Valenza, Compatible Consolidants from Particle-modified Gels, in: V. Fassina (Ed.), Proceedings of 9th International Congress Deterioration and Conservation of Stone 2, Elsevier, Amsterdam, 2000, pp. 459–465.
[93] X. Ouyang, D.A. Koleva, G. Ye, K. Van Breugel, Understanding the adhesion mechanisms between CSH and fillers, Cem. Concr. Res. 100 (2017) 275–283.
[94] E. Berodier, K. Scrivener, Understanding the filler effect on the nucleation and growth of C-S-H, J. Am. Ceram. Soc. 97 (2014) 3764–3773.